RMetS
Royal Meteorological Society

A seasonal and diurnal climatology of precipitation organization in the southeastern United States

Thomas M. Rickenbach,[a]* Rosana Nieto-Ferreira,[a] Christopher Zarzar[a] and Brian Nelson[b]
[a]*Department of Geography, Planning, and Environment, East Carolina University, Greenville, NC, USA*
[b]*NOAA/NESDIS, National Climatic Data Center, Asheville, NC, USA*

*Correspondence to: T. M. Rickenbach, Department of Geography, Planning, and Environment, East Carolina University, A-227 Brewster Bldg., Greenville, NC 27858-4353, USA. E-mail: rickenbacht@ecu.edu

This article describes results from a new four-year (2009–2012) radar-based precipitation climatology for the southeastern United States (SE USA). The climatology shows that a size-based classification between mesoscale precipitation features (MPF) and isolated precipitation reveals distinct seasonal and diurnal variability of precipitation. On average, from 70 to 90% of precipitation is associated with MPF, generally less in the summertime and in southern coastal regions. MPF precipitation has a relatively small seasonal cycle except in Florida and the warm offshore waters of the Gulf Stream. In contrast, isolated precipitation has a dramatic seasonal cycle that outlines the SE USA coastline whereas the MPF precipitation does not, consistent with a thermodynamic mechanism for onshore isolated storms in coastal regions. In summer, the isolated precipitation preferentially forms offshore at night, and dramatically 'flips' inland by early afternoon. In contrast, MPF precipitation has no clear diurnal variations except in the southern coastal region in the summer, likely associated with sea breeze convection organized on the mesoscale. These results suggest that the MPF versus isolated precipitation system framework provides a useful basis for future studies of large-scale and local controls on precipitation and resulting implications for long-range predictability of precipitation.

Key Words: precipitation; climate; diurnal; seasonal

Received 26 June 2014; Revised 20 November 2014; Accepted 24 November 2014; Published online in Wiley Online Library

1. Introduction

The southeastern United States (SE USA) is notable for a wide variety of precipitation regimes – mesoscale systems associated with baroclinic waves, cold-season frozen precipitation, tropical cyclones, and diurnally modulated local convection. Since the region is generally subtropical, these precipitation regimes are strongly modulated by the daily and seasonal cycle of solar radiation, locally generated convection, and baroclinic frontal precipitation. Appropriately, the SE USA has been the focus of many studies of precipitation variability, predictability and impacts (Konrad, 1997; Geerts, 1998; Hansen *et al.*, 1998; Carbone *et al.*, 2002; Parker and Ahijevych, 2007, Shepherd *et al.*, 2007).

This article describes results from a four-year surface radar-based precipitation climatology for the SE USA, that addresses whether a simple size-based classification of precipitation features can reveal key differences in seasonal and diurnal variability of precipitation. This approach is different from existing climatologies that emphasize convective versus stratiform precipitation (Schumacher and Houze, 2003). Separation of convective and stratiform precipitation has been used to quantify the impact of distinct modes of diabatic heating on atmospheric circulations, whereas the present climatology relates to the reverse connection – the impact of atmospheric circulation on precipitation. Large-scale features of the atmospheric circulation are better represented and more accurately reproduced in climate models compared to precipitation (Kalnay *et al.*, 1996). Accordingly, one approach to improving precipitation predictability in climate models is to distinguish between precipitation systems associated with more predictable large-scale features of the atmospheric circulation and precipitation associated with less predictable local processes. This article is a first step toward that goal, by examining for the SE USA distinct seasonal and diurnal variations of precipitation organization that may suggest differences in forcing mechanisms.

It has been recognized over the past several decades that the spatial scale of precipitation system organization, as measured by weather radar, has some relation to precipitation forcing mechanisms (e.g. mesoscale–synoptic-scale versus local-scale forcing). The pioneering work of Leary and Houze (1979), using shipboard radar observations of precipitation systems in the tropical eastern Atlantic, established a paradigm of the radar-observed mesoscale precipitation feature (MPF) as being associated with larger-scale dynamical forcing (in that case, tropical easterly wave troughs). In the midlatitudes, such forcing includes the frontal regions of extratropical cyclones, as well as synoptic-scale ascent associated with the divergent region of a jet stream trough (Houze *et al.*, 1990; Laing and Fritsch, 2000; Parker

and Johnson, 2000). These and other studies of tropical and warm-season subtropical precipitating cloud systems (e.g. Cheng and Houze, 1979; Gamache and Houze, 1983; McAnelly and Cotton, 1989; Alexander and Young, 1992; Steiner *et al.*, 1995) emphasized MPFs of convective origin, which came to be known as mesoscale convective systems (MCS). The MCS is defined (Houze, 1989, 2004) as a contiguous region of precipitation of convective origin at least 100 km in horizontal dimension. In the Tropical Rainfall Measuring Mission (TRMM) era, surface and space-borne assets including radar and passive microwave radiometer (Mohr and Zipser, 1996; Rickenbach and Rutledge, 1998; Nesbitt *et al.*, 2000, 2006; Schumacher and Houze, 2003) have shown that MCS are the dominant unit of tropical precipitation.

When generalizing precipitation organization beyond tropical and warm-season rain to the higher latitudes, including winter precipitation, it is useful to consider the more general construct of an MPF, which, as applied herein, does not constrain precipitation to be necessarily of convective origin. In this regard, an MCS may be thought of as a subset of MPF composed in part of convective rain, noting that the MCS definition of Houze (1989) does not specify a convective rain fraction threshold. For example, in the southeastern USA, MCS have been shown to be most common generally in the spring and early summer, since at that time of the year the combination of baroclinicity and thermodynamic instability are greatest in that region (Geerts, 1998). Yet, the relative contribution of frozen precipitation to the annual precipitation climatology in the subtropical SE USA has not received much attention. This suggests that the MPF, with no requirement of convective origin for precipitation, is an appropriate construct in studying year-round precipitation outside the Tropics.

Rain features of smaller scale than MPF, that is, isolated precipitation systems, tend to form in response to local-scale circulations such as the sea breeze, topographic circulations, or thermal circulations in the boundary layer, modulated by the diurnal cycle of solar radiation (Wallace, 1975). Though isolated systems are not uniquely associated with either local or large-scale forcing, in certain regimes isolated precipitation systems may account for a larger fraction of the precipitation climatology. Rickenbach and Rutledge (1998) showed that for an oceanic location in the equatorial western Pacific, isolated convective systems accounted for about 15% of the precipitation during a three-month field campaign, concentrated in periods when the suppressed phase of equatorial waves resulted in fewer large convective systems. Due to their small spatial scale and dependence on complex surface energy fluxes, processes controlling thermodynamically forced precipitation are more crudely represented in forecast and climate models. For example, there remains a persistent early bias in the diurnal timing of precipitation in general circulation models (GCM), as most cumulus parametrization schemes exhaust convective available potential energy (CAPE) as soon as it occurs, leading to diurnal rainfall maxima several hours earlier than observed (Pritchard and Somerville, 2009). New breakthroughs to improve the diurnal precipitation phase and amplitude produced by GCM cumulus parametrizations (Chao, 2013) may benefit from observational validation such as that presented here.

This article presents a four-year climatology (2009–2012) of precipitation from MPF and isolated precipitation systems across the southeastern USA, based on a high-resolution national surface radar composite dataset. The goal of the article is to determine whether and how the seasonal and diurnal variations of MPF versus isolated systems are distinct. These results will form a basis for future studies of large-scale and local controls on precipitation and resulting implications for long-range predictability of precipitation. Section 2 describes the radar-based National Mosaic and Multi-sensor Quantitative Precipitation Estimation (NMQ) radar reflectivity and precipitation datasets (Zhang *et al.*, 2011) along with the implementation of MPF and isolated system identification. Section 3 presents the seasonal cycle and geographic distribution of both types of precipitation organization. In section 4, the diurnal variation of precipitation organization is analysed regionally and seasonally. Conclusions and next steps are offered in section 5.

2. Methods and examples

The National Oceanic and Atmospheric Administration (NOAA) National Severe Storms Laboratory (NSSL), in conjunction with the University of Oklahoma and others have developed high-resolution precipitation and radar reflectivity datasets for the contiguous United States, based on the national network of Next-generation Doppler Radars (NEXRAD). These are the National Mosaic and Multi-sensor Quantitative Precipitation Estimation (NMQ – 'Q2') precipitation dataset, and the corresponding radar reflectivity field (NMQ - 'Mosaic-2D') that includes precipitation phase and type (Zhang *et al.*, 2011). The dataset covers the contiguous United States, extending approximately 200 km offshore in the southeastern USA. In a few regions where NEXRAD coverage is not optimal, data from terminal Doppler weather radars (TDWR) and other gap-filling radar systems are ingested. In mountainous terrain, use of adjacent radars and multiple elevation angle scans are optimized to mitigate the inevitable beam blockage problems. The NMQ system was placed in a high-resolution (1 km × 1 m × 5 min) set of multisensory precipitation products (Prat *et al.*, 2010) and generated at the National Climatic Data Center (NCDC), which we utilize in the present study. The Q2 is a radar-based precipitation product that incorporates surface and radar observations to provide a state-of-the-art estimation of precipitation rate. Mosaic-2D contains the corresponding quality-controlled radar reflectivity field, with precipitation separated into convective and stratiform components (Steiner *et al.*, 1995), and flagged as liquid or

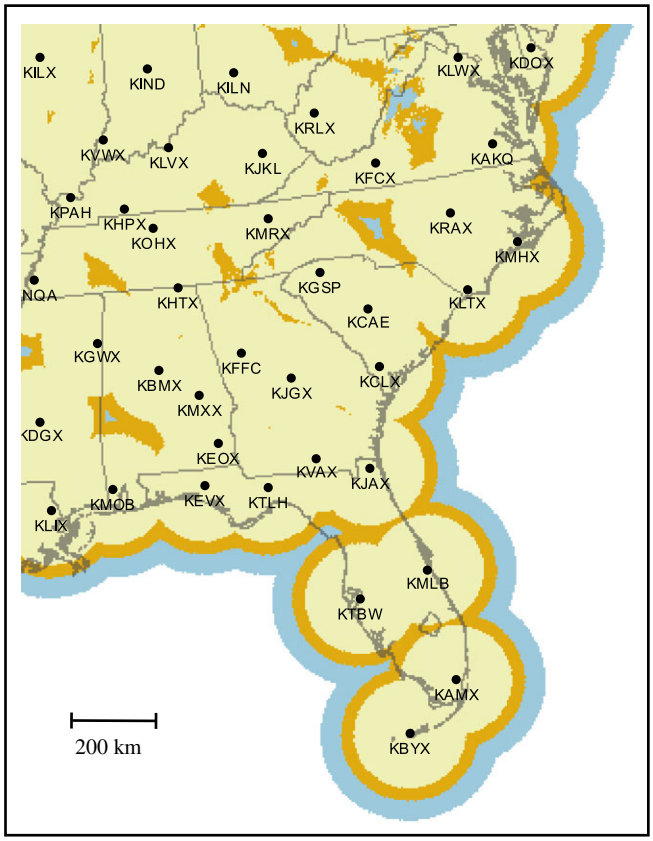

Figure 1. The network of NEXRAD radars and the domain over the southeastern USA used in this study. Range of radar coverage starting at 3 km above the surface shown in grey (blue in online; 1.8 km in dark grey; orange in online and 1.2 km in light grey; yellow in online), due to the increasing height with range of the radar beam at the lowest scanning angle. Adapted from NOAA National Weather Service Radar Operations Center website (http://www.roc.noaa.gov/WSR88D/).

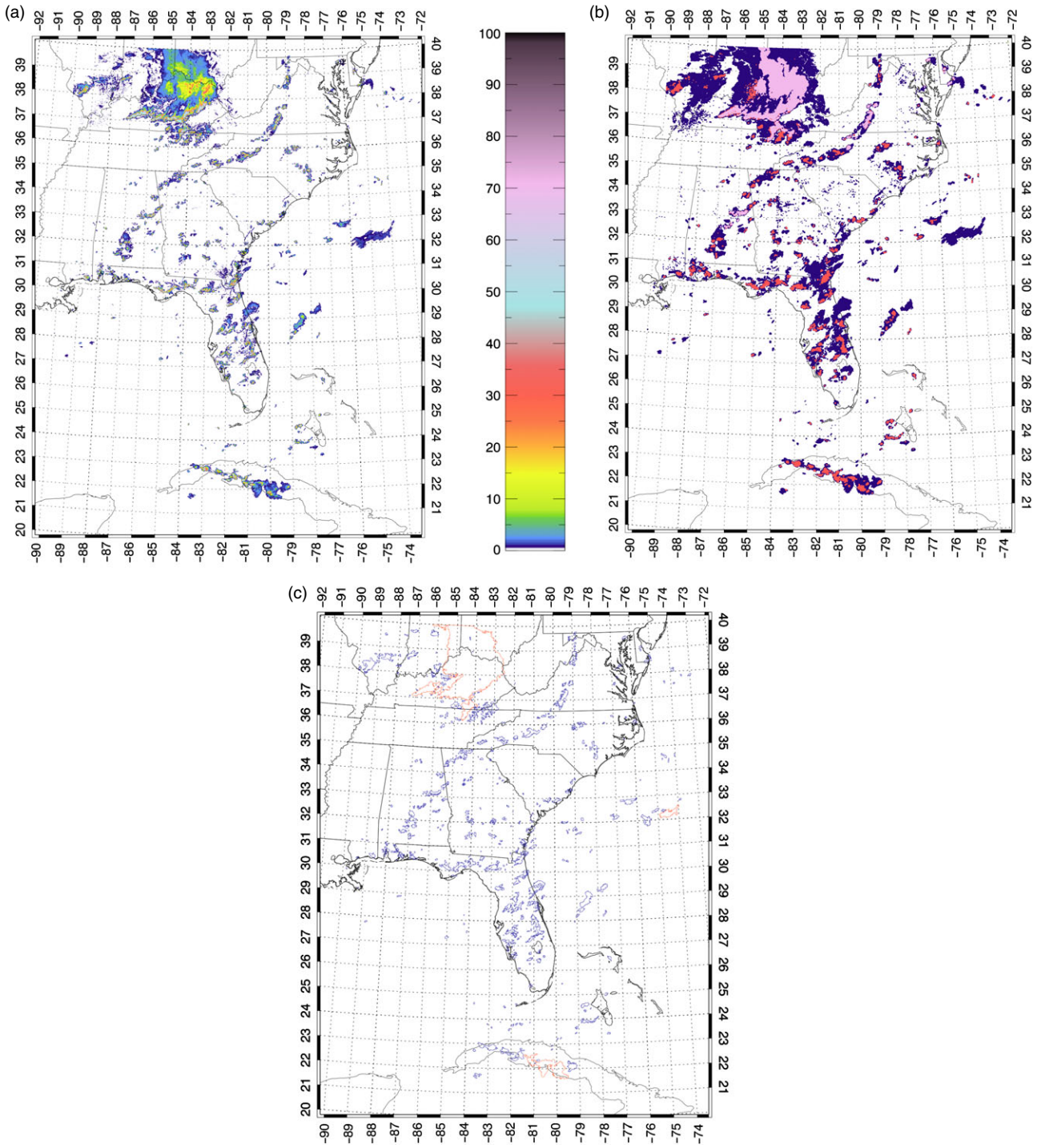

Figure 2. Example on 4 August 2009, 2030 UTC of (a) instantaneous rain rate (mm h^{-1}), (b) precipitation type from the NMQ data, and (c) MPF and isolated precipitation features >0.5 mm h^{-1} based on analysis of contiguous feature size. MPF features are shown in light grey (red in online), with isolated features shown in dark grey (blue in online). Precipitation types shown are tropical rain (light grey shading; pink in online), convective rain (dark grey shading; red in online), stratiform snow (off white shading; green in online), and stratiform rain (black shading; blue in online).

frozen precipitation based on the position and structure of the radar bright band and the vertical profile of temperature from model-derived sounding data. Though both products are extensively quality-controlled (Zhang *et al.*, 2011), inevitable limitations remain such as range issues affecting beam blockage and resolution that impact uniform coverage of the radar scans as well as the determination of precipitation type.

To construct the MPF and isolated system precipitation climatology, we extracted the Q2 and Mosaic-2D data over the southeastern USA, from Louisiana to the Ohio Valley in the west, and from south Florida to Chesapeake Bay in the east. The range of NEXRAD coverage over the ocean extends approximately 200 km from the coastline (Figure 1). There are three regions (western Virginia, western North Carolina, and western Alabama) where limited overlapping coverage, mountainous terrain or both required use of radar reflectivity up to 3 km above the surface. In the NMQ dataset, the western North Carolina region was supplemented by TDWR radar, 'filling in' most of the coverage in that area (NOAA Radar Operations Center (ROC)).

The climatology was constructed by producing daily averages of MPF and isolated system rainfall, then compositing the daily averages into seasonal and annual means. For the daily averages, data was analysed at a 15 min interval, rather than the native 5 min interval of the data, to reduce high demands on processing resources without sacrificing sufficiently high temporal resolution to adequately capture precipitation variability on daily and longer time-scales. Both Q2 and Mosaic-2D were ingested simultaneously into a fully automated processing system. For each 15 min snapshot, all contiguous precipitation features were identified and thresholded at 0.5 mm h^{-1} (about 18 dBZ, roughly light

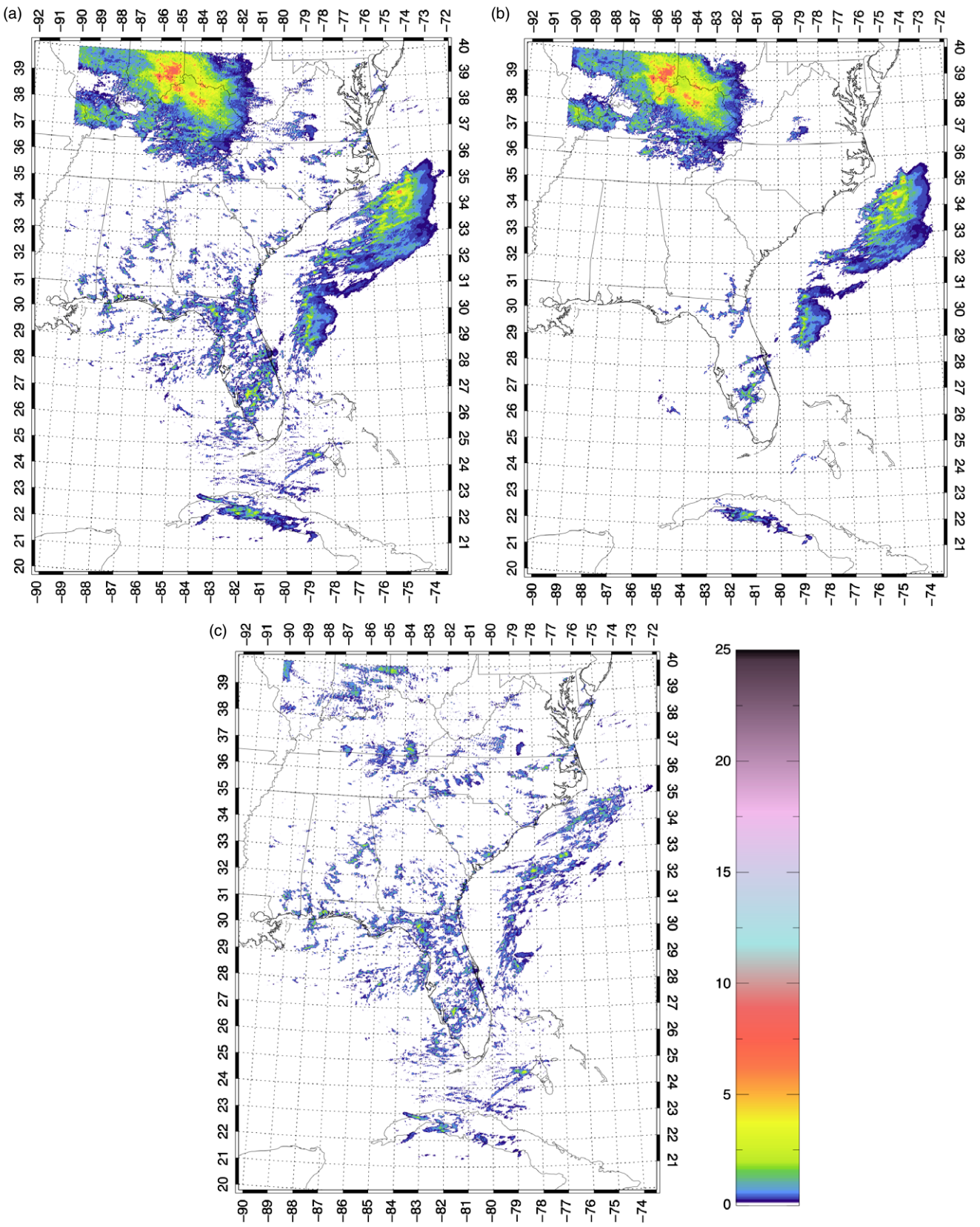

Figure 3. Daily mean precipitation rate (mm day^{-1}) on 4 August 2009 for (a) total rainfall, (b) the portion of total rain associated with MPF, and (c) the portion of total rain associated with isolated systems.

drizzle intensity) to ensure that any residual non-meteorological artefacts in the NMQ product were not included. The maximum length of each feature in the domain was determined, with those features exceeding 100 km in length placed into the MPF category with the remainder of features placed into the isolated systems category, conceptually following Rickenbach and Rutledge (1998) and Nesbitt *et al* (2006). Precipitation features were not tracked in time but determined independently from each 15 min snapshot, then integrated into daily averaged maps at 1 km pixel resolution of precipitation rate. From the daily averaged maps, seasonal and annual composite maps were produced. For the diurnal analysis, the precipitation organization analysis data were saved every 3 h on the hour, and composited seasonally and annually.

To illustrate the implementation of the MPF vs. isolated system climatology, two examples are presented for typical summer and winter days. The Q2 precipitation map for 4 August 2009 at 2030 UTC (Figure 2) shows an MPF moving eastward across the

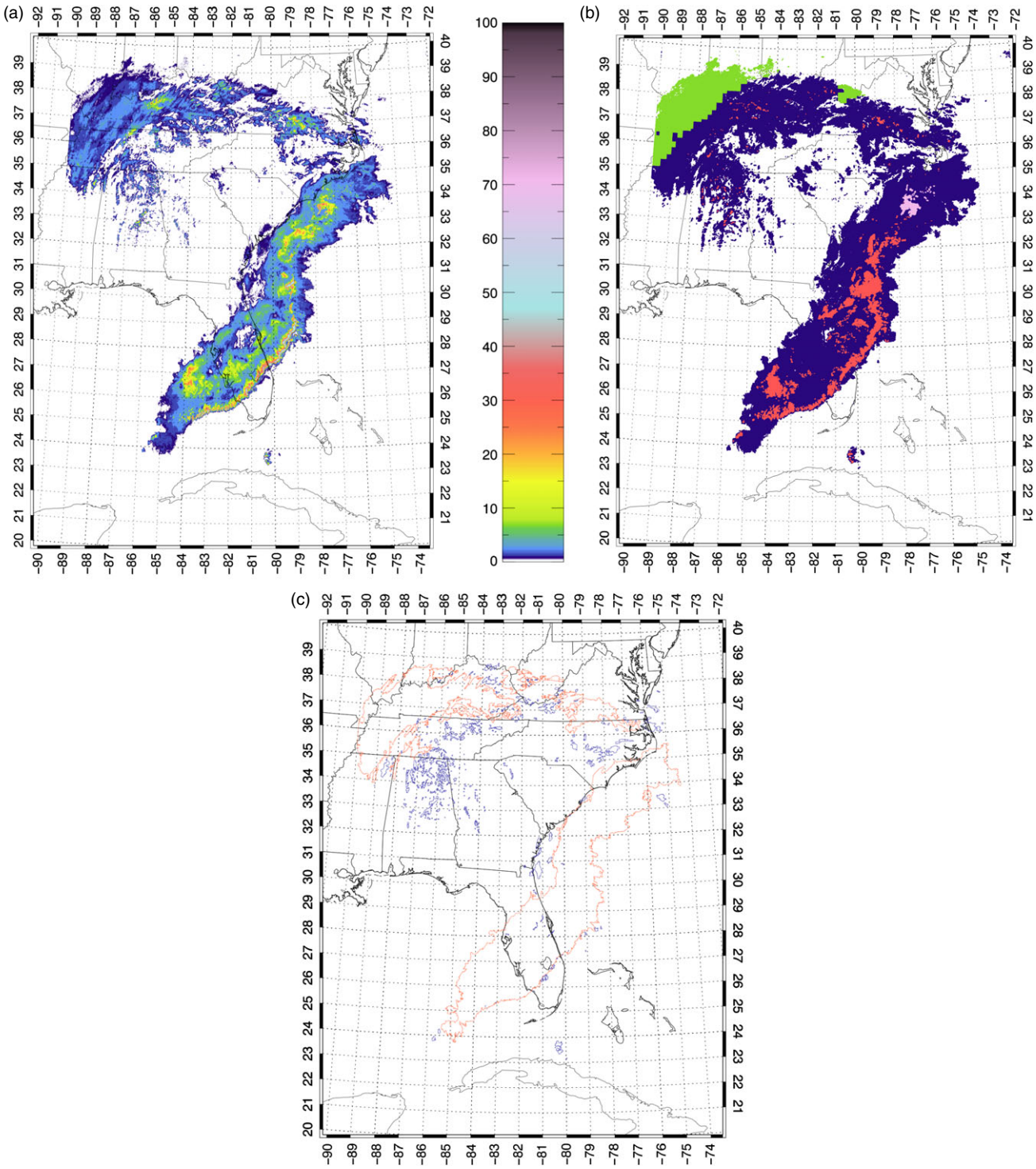

Figure 4. As in Figure 2, but for 26 January 2011, 0230 UTC.

Ohio Valley with a leading edge of convective cells and extensive embedded convection within the trailing stratiform rain area (a 'classic' MCS). Scattered isolated convective cells occur across the SE USA, concentrated in Florida along the coastal region, as is common on summer afternoons. The Mosaic-2D product provides the corresponding precipitation type, primarily convective rain cores surrounded by stratiform rain. The convective rain in the MPF is further classified by the NMQ algorithm as 'tropical', indicating minimal rain evaporation below the 0 °C level as inferred from the vertical profile of reflectivity at those pixels (Xu *et al.*, 2008). If the maximum distance between border points of each contiguous precipitation feature is greater than 100 km, all pixels within those features are identified as MPF while all smaller features are flagged as isolated systems. For example, Figure 2 identifies three features as MPF: the large system in the Ohio Valley, a merging group of convective cells over Cuba, and the remnant of a dissipating MCS off the South Carolina coast near the ∼200 km (1.5°) range limit of the coastal radars. Precipitation maps like these were similarly analysed at 15 min intervals to produce the daily averaged maps of MPF, isolated and total precipitation for 4 August 2009 (Figure 3). From the total daily averaged map, the two widespread rain regions (the Ohio Valley and offshore from the southeast coastal plain) are associated with MPF, while scattered isolated rain occurred across the entire domain, concentrated along the Florida coast. The daily-mean precipitation maps show the scattered heterogeneous spatial pattern of isolated rain systems, in contrast to the widespread rainfall associated with each MPF.

A contrasting example is a wintertime extratropical cyclone that occurred on 26 January 2011 (Figure 4). The precipitation pattern at 0230 UTC reveals the 'comma' shape typical of an extratropical cyclone, with a large squall line MCS in the warm sector from

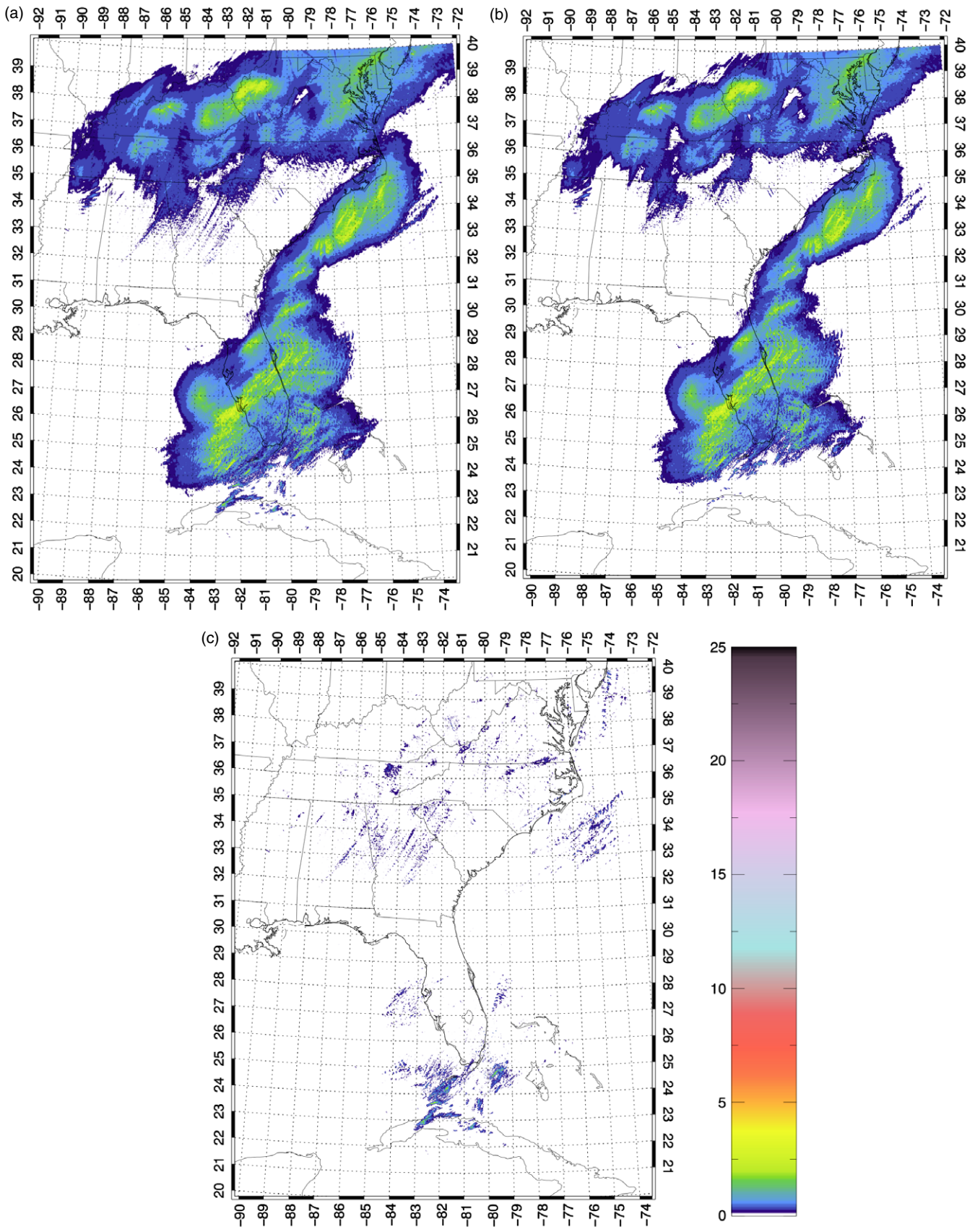

Figure 5. As in Figure 3 but for 26 January 2011.

the Gulf of Mexico to North Carolina and lighter precipitation wrapping around the cyclone centre in northern Alabama. The precipitation in the warm sector is convective on the leading edge of the MCS with trailing stratiform rain. North of the cyclone centre light stratiform rain gives way to frozen precipitation in the northwest quadrant. The feature analysis identifies four large MPF. The largest, a squall line MCS, extends over 1000 km from eastern Virginia to the radar domain limit north of western Cuba, while the others in the northern domain are large areas of stratiform rain with weak embedded convection. The isolated rain systems identified across the region are characterized by weak convective cells or small areas of light rain. The daily mean precipitation maps for the winter case (Figure 5) reveal that most of the precipitation was associated with MPF, with light isolated precipitation features moving generally to the northeast with the propagating cyclone.

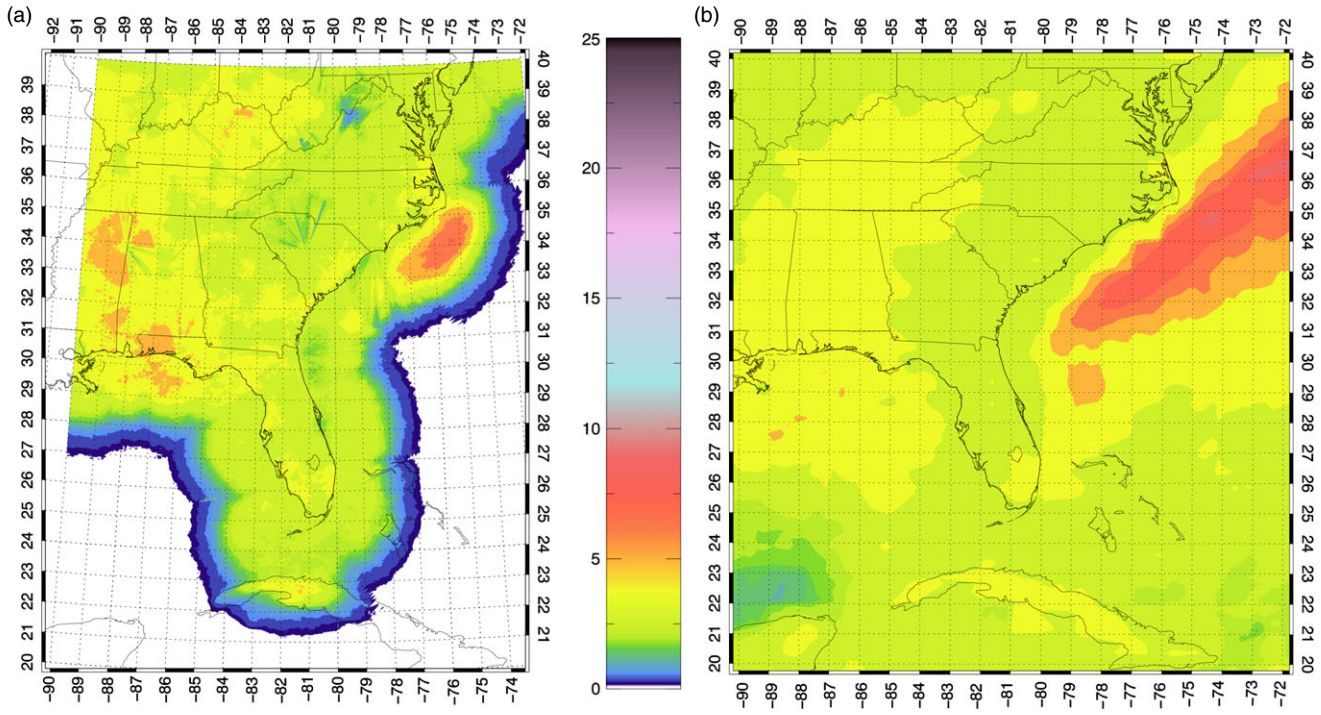

Figure 6. The 2009–2012 average precipitation (mm day^{-1}) from (a) the NMQ radar product and (b) the TRMM satellite 3B-42 product.

These contrasting examples of summer and winter precipitation demonstrate that the analysis approach is able to distinguish between the distribution and structure of MPF and isolated systems. Next we examine the four-year annual mean and seasonal cycle climatologies.

3. Four-year climatology of precipitation organization

We begin with a comparison of the general features of the four-year (2009–2012) mean climatology of precipitation across the SE USA between the NMQ product and the satellite-based TRMM 3B-42 climatology for the same area (Figure 6). These two independent datasets are quite consistent with each other, both with a similar pattern and magnitude of precipitation. The conspicuous features of the climatology include the higher precipitation amounts over land east of the Mississippi River and lower amounts on the lee (east) side of the Appalachian Mountains to the coastal plain. Precipitation associated with the warm Gulf Stream current increases dramatically just off the Atlantic coast south of the North Carolina Outer Banks barrier islands (Cape Hatteras) and down to the northeast coast of Florida. Note the range limit of the NMQ product to about 200 km offshore, as well as two small regions of reduced data coverage, due to blockage of the radar beam and limited NEXRAD coverage, in northwestern South Carolina and in the northwest corner of Virginia.

3.1. *Southeastern US overview*

The 2009–2012 climatology of MPF and isolated precipitation (Figure 7) reveals important contrasts between the two precipitation types. The MPF rain distribution looks very much like the total precipitation (Figure 6(a)), consistent with the observation from Figure 7(c) that 70–90% of the precipitation over the Mississippi and Ohio river valleys, as well as the coastal plain, belongs to the MPF category. A relative minimum in MPF precipitation can be seen in the lee (east) of the Appalachian high country in the Carolinas. This is broadly consistent with the observation by Parker and Ahijevych (2007) that eastward-moving warm-season MCS tend to weaken over the Appalachians and re-strengthen or re-form over the Piedmont region. In contrast, isolated precipitation occurs in much lower quantity across the entire domain, but is concentrated in four regions (in order of increasing amount): the southeastern Atlantic coast, the Gulf Stream off the Carolina coast, the Florida Gulf Coast, and the southern Florida peninsula. Isolated precipitation outlines the SE USA coast whereas the MPF precipitation does not, consistent with a thermodynamic mechanism for onshore isolated storms in coastal regions. Note also that the fraction of MPF precipitation is a relative minimum along the immediate SE USA coast and across the Florida peninsula. Though coastal precipitation in the SE USA has been studied in previous climatologies (Wallace, 1975; Carbone and Tuttle, 2008; Prat and Nelson, 2014), our results associate the coastal rain generally with isolated storms, not MPF. Coastal isolated precipitation will be explored further in section 4.

The 2009–2012 mean seasonal cycle of MPF precipitation (Figure 8) illustrates that although MPF precipitation occurs across the SE USA throughout the year, there are notable regional differences. The most extensive MPF precipitation occurs in springtime (MAM) in the southern Ohio Valley, western Tennessee and Mississippi. This observation is consistent with a 15-year climatology (Ashley *et al.*, 2003) of mesoscale convective complexes (long-lived warm-season MCS) showing a monthly precipitation maximum in that region in springtime (May), migrating northward to the upper Midwest during the summer. The Appalachian region from western Virginia to the western Carolinas has a summertime (JJA) minimum. Parker and Ahijevych (2007) documented a regional minimum in warm season MCS occurrence in the southern Appalachian high country, which they attributed to the disruption of MCS circulations by the mountain ridges as MCS approach from the west. In addition, persistent troughs of low pressure downstream of the Appalachians favour MCS initiation or resurgence to the east of the mountains (Koch and Ray, 1997). In southern and central Florida, MPF rainfall increases from a winter (DJF) minimum to a summertime (JJA) maximum that extends both over the land and ocean. Although the Gulf Stream MPF rainfall maximum off the Carolina coast persists year round, the MPF rainfall is greatest during summer (JJA) and autumn (SON), at nearly twice the wintertime amount.

The seasonal cycle of isolated precipitation (Figure 9) is quite marked, in contrast with the weak seasonal cycle of MPF. In winter (DJF) isolated precipitation is nearly absent except for over the ocean off the southern and eastern Florida coast up to the Carolinas, which coincides with the relatively high wintertime sea-surface temperatures (SSTs) (Figure 10(a)) along the Gulf Stream

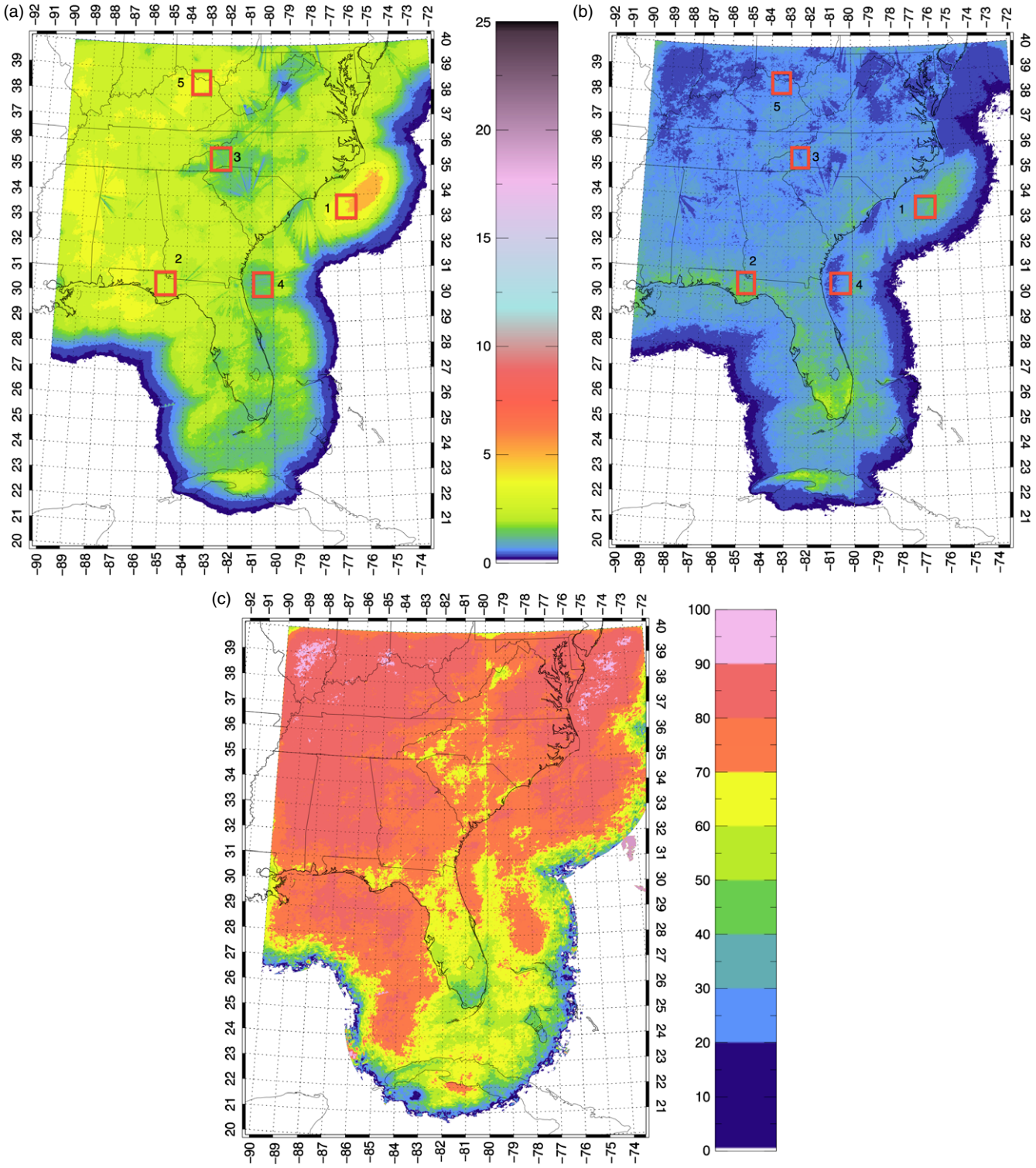

Figure 7. The 2009–2012 average precipitation (mm day^{-1}) from the NMQ product for (a) MPF precipitation, (b) isolated precipitation, and (c) the percentage of total precipitation in the MPF category. 1° × 1° box locations in (a) and (b) show regions for further analysis later in the article and are as follows: box 1 – Gulf Stream off North Carolina southeast coast, 33°N–34°N, 76°W–77°W; box 2 – Florida panhandle 30°N–31°N, 84.5°W–85.5°W; box 3 – western North Carolina 35°N–36°N, 82°W–83°W; box 4 – offshore of Georgia–north Florida coast 30°N–31°N, 80°W–81°W; box 5 – Ohio Valley 38°N–39°N, 83°W–84°W.

near the SE US coast. In spring (MAM) isolated precipitation increases across the domain, particularly in southern Florida. The summer (JJA) pattern clearly shows the outline of the entire SE coast, the warm Gulf Stream current, and the island of Cuba. The isolated precipitation generally decreases to the north and also decreases away from the coast. A very strong isolated rain gradient over the ocean north of 35°N latitude (Cape Hatteras, North Carolina) corresponds to the sharp climatological decrease in SST as the Gulf Stream is directed northeastward by the coastal contour, away from land. There is an interesting summertime 'rain shadow' over the ocean within 100 km of the Georgia and northern Florida coast, which is also clearly visible in TRMM satellite 3B-42 rain climatologies (Prat and Nelson, 2014). This feature is most evident in the isolated precipitation maps (rather than the MPF maps), primarily during spring and summer. There is a climatological minimum of SST along the southeastern coast (Figure 10), from Florida to North Carolina, in generally the same region. However, the precipitation minimum is most evident in the summer, the season when the SST minimum and associated SST gradient is smallest. Yet the location and season suggest that the precipitation minimum is related to a land–ocean heating contrast in some way. In the autumn months (SON) the isolated precipitation greatly decreases across the domain, but persists in south Florida and along the Gulf Stream where the

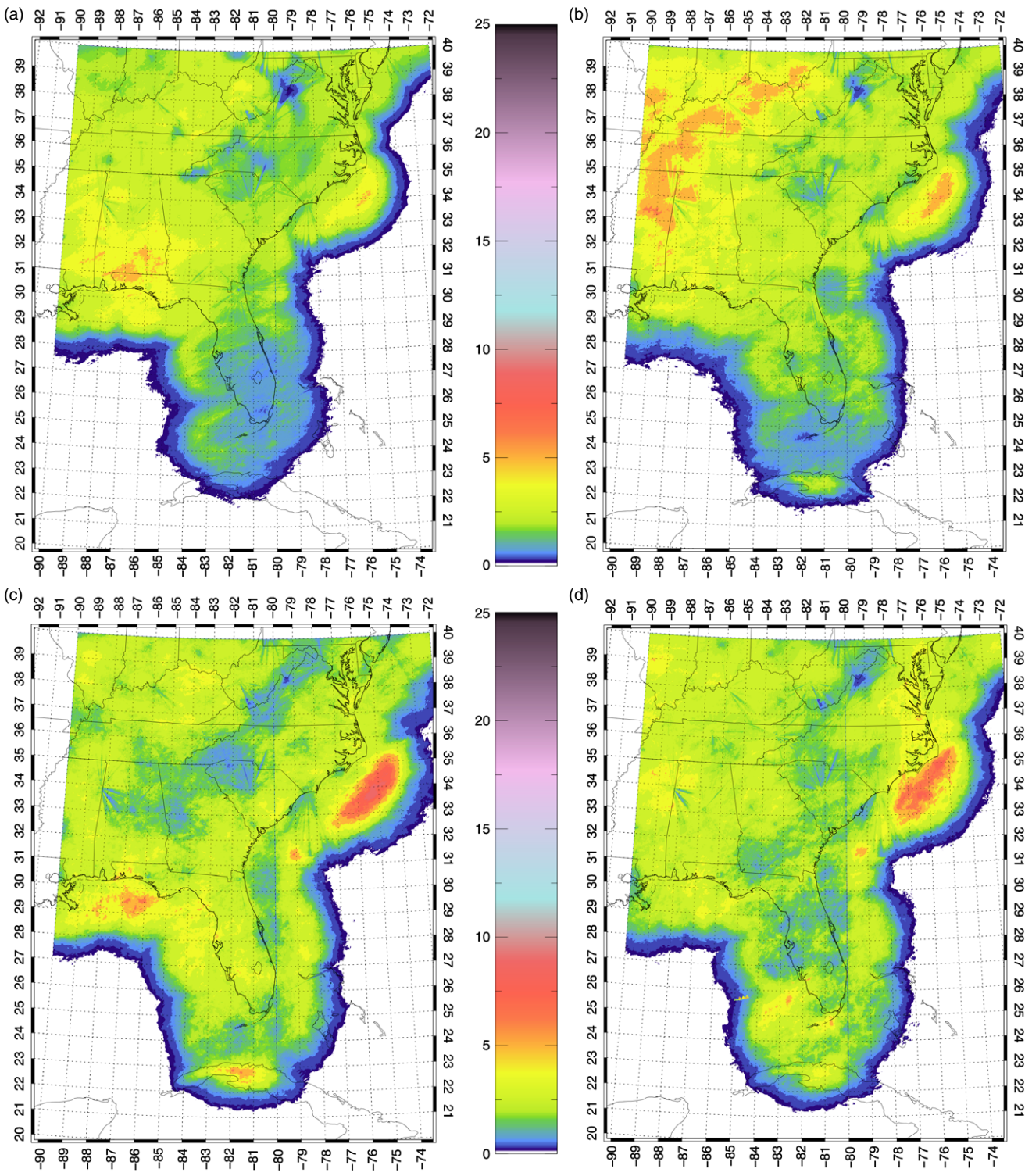

Figure 8. The 2009–2012 seasonally averaged MPF precipitation (mm day^{-1}) from the NMQ product for (a) DJF, (b) MAM, (c) JJA, and (d) SON.

SSTs remain near their summertime values. In summary, the annual cycle of isolated precipitation appears rather clearly to be thermodynamically driven, suggesting that isolated rain responds to surface heating either directly through high moisture content and thermodynamic instability, or indirectly through thermal circulations such as the sea breeze, or both.

3.2. *Regional differences*

These results indicate that in addition to the general SE USA characteristics of the annual cycle of precipitation, there are important regional differences that provide some insight with respect to mechanisms controlling seasonal changes in precipitation. Five 1° × 1° boxes were chosen for analysis (box locations shown in Figure 7), based on qualitative differences in regional precipitation noted in the previous discussion. These regions include ocean and land, coastal and inland locations, as follows: the Gulf Stream off the southeast coast of North Carolina (box 1), the Florida panhandle (box 2), western North Carolina (box 3), offshore from the Georgia–north Florida coast (box 4), and the Ohio River Valley (box 5). Figures 11 and 12 present the four-year-averaged seasonal means of isolated and MPF precipitation, along with the fractions of the total precipitation and time present for MPF, for these five regions. The Gulf Stream off the southeast Carolina coast (box 1) has the highest annual-mean precipitation of any region in the SE USA (cf. Figure 6), with the MPF precipitation contributing up to 90% of the total winter precipitation and down to 71% in the summer (Figure 12). Kuwano-Yoshida *et al* (2010), in a modelling study of the precipitation response to the warm Gulf Stream, suggested that deep atmospheric vertical

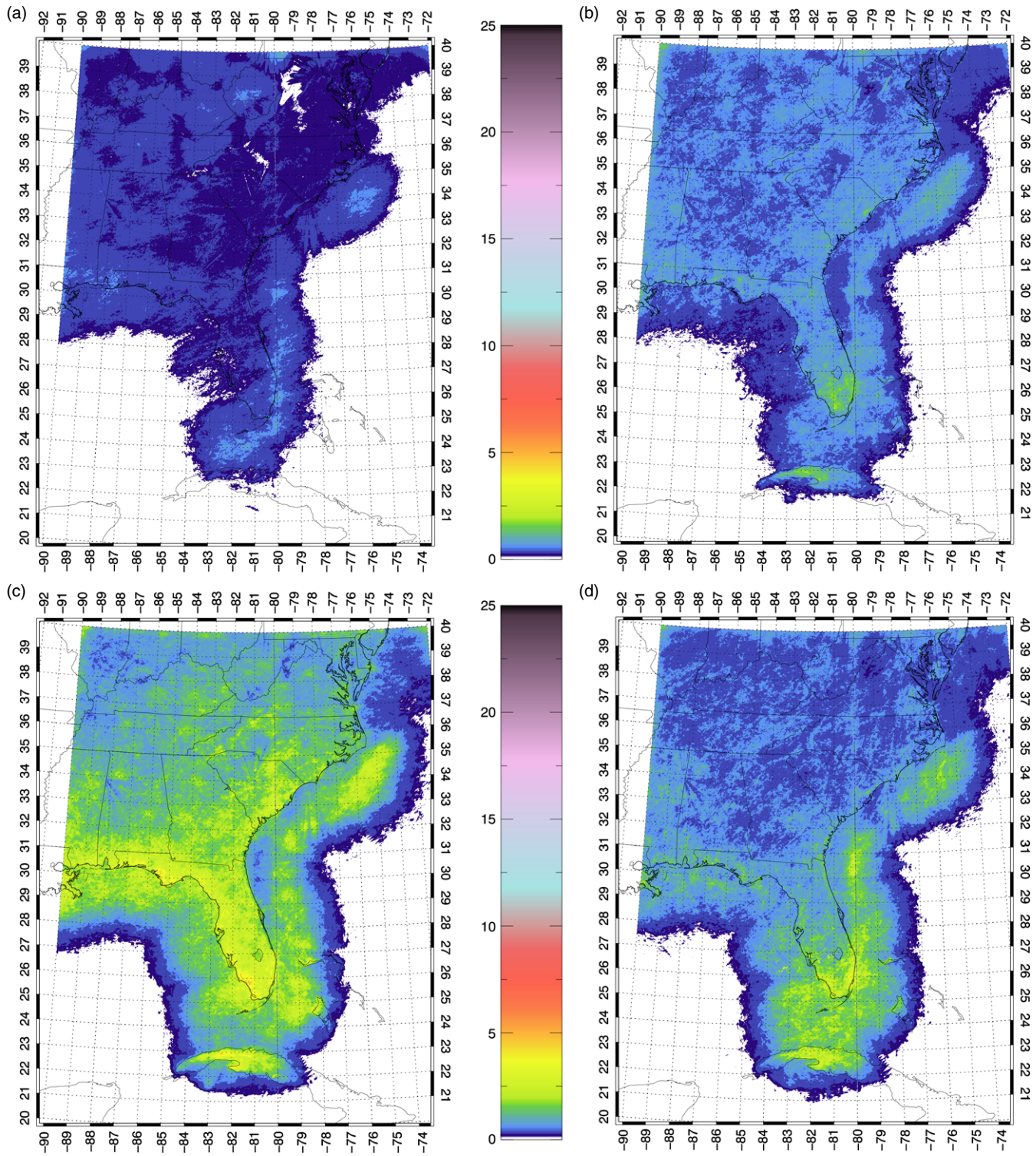

Figure 9. As in Figure 8 but for isolated precipitation.

circulations are driven by SST gradients (perhaps once SSTs reach a certain threshold value), favouring widespread summertime precipitation systems over the Gulf Stream. Along the Gulf Stream off the Carolina coast the MPF precipitation increases steadily from winter to autumn (Figure 11(a)), while MPF are most common in the autumn. Although during autumn (SON) that region is generally impacted by both tropical and baroclinic systems, there were only two tropical systems off the Carolinas during the 2009–2012 period (Tropical Storm *Beryl* in late May 2012, and Hurricane *Irene* in August 2011). The maximum MPF activity during autumn in that region is possibly related to seasonally high SSTs (25–26 °C) combined with a large SST gradient (Figure 10(d)). There is a clear summer (JJA) maximum in the isolated precipitation (Figure 11(b)) in all regions except the rain shadow off the Georgia coast, strongly suggesting a general thermodynamic enhancement of local precipitation over warm land and ocean in the summertime. Over the Florida panhandle along the Gulf coast, MPF rainfall decreases from spring to autumn by nearly a factor of 2. In the summer (JJA), isolated rain along the Florida panhandle makes up over half (57%) of summer rainfall in that region. Western North Carolina is situated in the Appalachian high country, where Parker and Ahijevych (2007) have documented a minimum in MCS occurrence as discussed earlier. The low amount of MPF precipitation in western North Carolina shown in Figure 11 is consistent with that finding. Isolated precipitation also makes up over half of the total summertime rain in that region. The Ohio Valley has maximum MPF precipitation in the spring and summer with just over 90% of springtime precipitation in the MPF category, decreasing to 78% in the summer as isolated rain increases. Aside from the

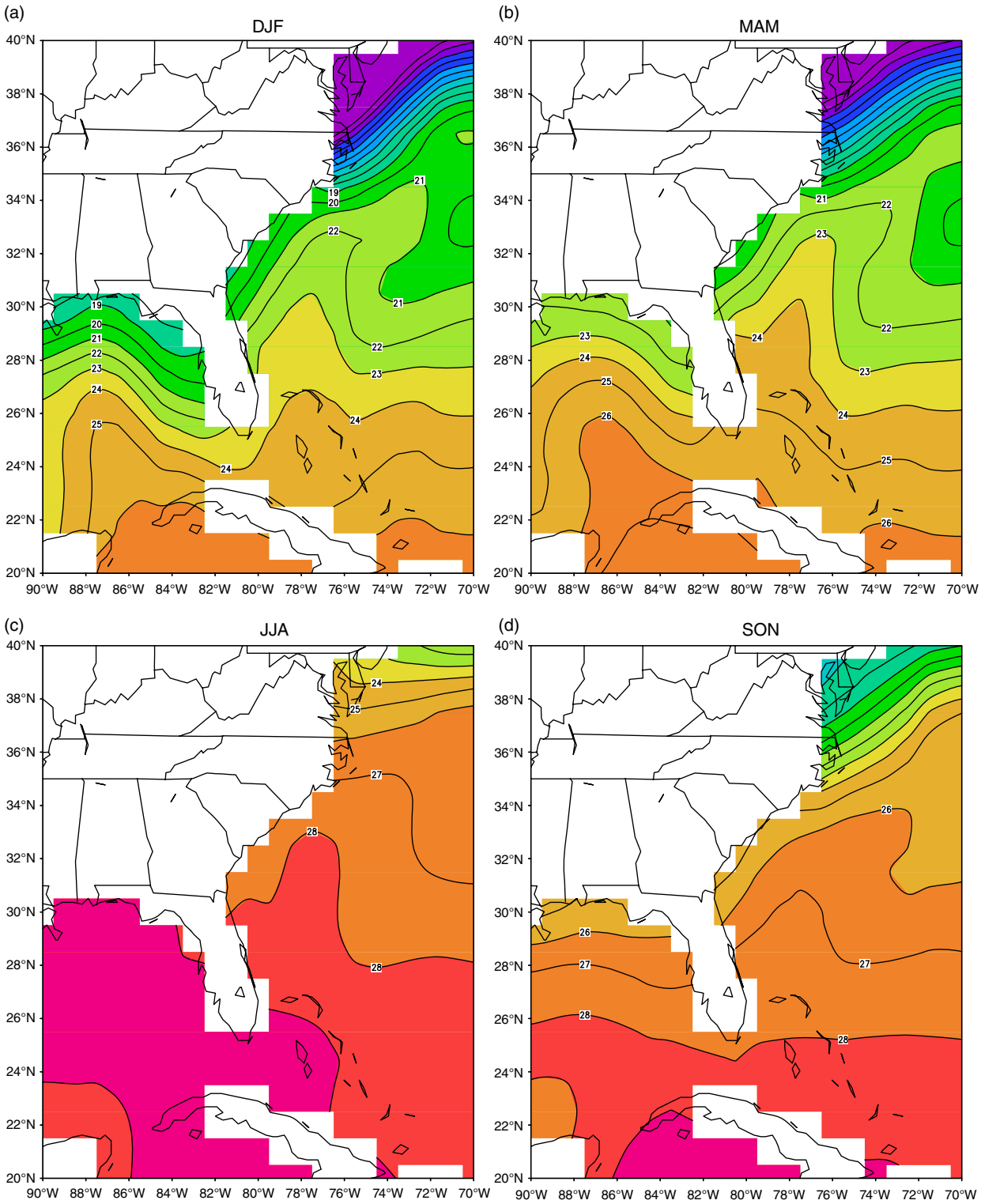

Figure 10. The 2009–2012 seasonally averaged sea-surface temperatures for (a) DJF, (b) MAM, (c) JJA, and (d) SON. Contour interval is 1 °C. Data are from the 1° global NOAA Optimum Interpolation SST Product (V2), available at http://www.esrl.noaa.gov/psd/data/gridded/data.noaa.oisst.v2.html.

Gulf Stream, MPF precipitation is most common in winter and spring (Figure 12(b)), in particular the Ohio Valley to the north. Nieto-Ferreira *et al* (2013) show that the seasonal changes in extratropical cyclone precipitation across the SE USA are quite similar to the seasonal pattern of MPF precipitation shown herein, suggesting a strong association of MPF with baroclinic forcing. Taken together, these observations suggest that farther north the isolated precipitation regime generally yields to a baroclinic regime in the autumn and winter dominated by MPF, while farther south isolated precipitation dominates into the summer season.

The annually-averaged (2009–2012) time series of daily-mean precipitation (Figure 13), averaged over each of the five boxes, shows the annual precipitation cycle of those five regions in more detail. Though all regions have clear warm-season maxima in isolated rain, the duration, amplitude and timing show regional differences. The Gulf Stream off the Carolina coast has a broad maximum in isolated precipitation from March to November, while in contrast the coastal Florida panhandle has a shorter May–October isolated rain season with a larger and more peaked August maximum. Off the Georgia–Florida coast (box 4, Figure 13) there is an indication of two seasonal isolated precipitation maxima – June/July (smaller) and October (larger). Over the Gulf Stream, the extremes in MPF precipitation are scattered evenly throughout the year, reaching values up to about three times the 'background'. The lack of a clearly defined seasonal cycle of MPF precipitation is common to all regions,

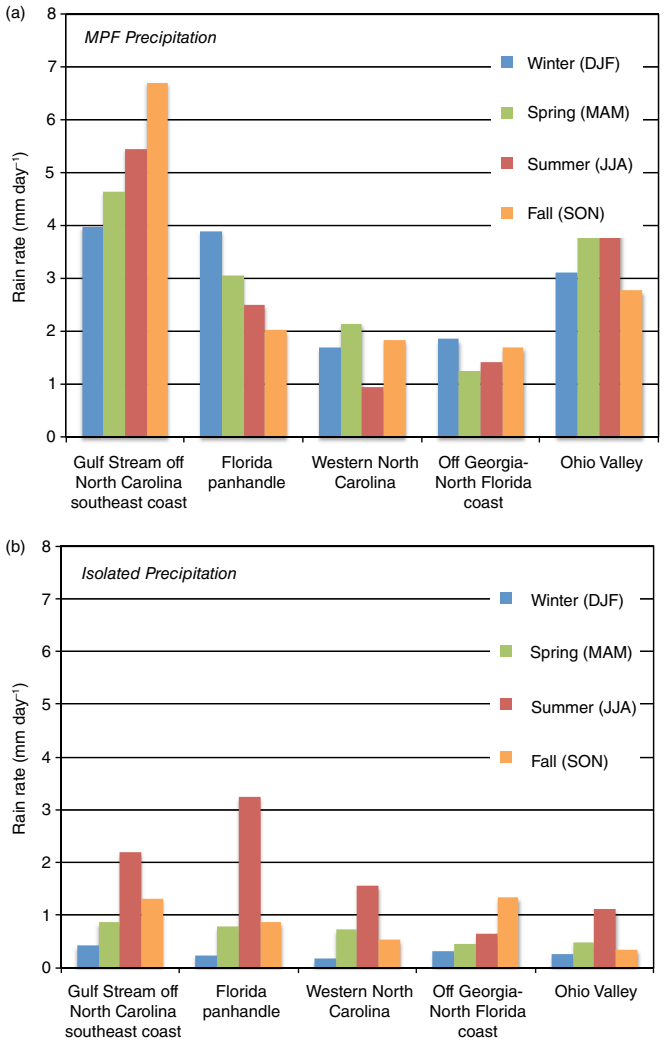

Figure 11. The 2009–2012 seasonally averaged precipitation (mm day^{-1}) for (a) MPF and (b) isolated within the five 1° × 1° boxes shown in Figure 7.

illustrating that there are both warm and cold season regimes of organized precipitation. In the Ohio Valley, there is an indication of two seasonal maxima of MPF precipitation – May (spring) and August (summer). To quantify the regional differences in extreme precipitation, Tables 1 and 2 give the 2009–2012 frequency distributions of daily-mean precipitation (isolated and MPF separately) for each of the five box regions. The Florida panhandle has the largest tail of mid-to-high-range daily averaged isolated precipitation, consistent with strong thermodynamic forcing from strong coastal solar heating combined with a constant moisture source from the Gulf of Mexico. In contrast, the distribution is shifted to lighter isolated precipitation in the western Carolina high country. For MPF precipitation, the Gulf Stream off the Carolina coast has the broadest distribution of daily-mean values, while the distribution is shifted to more frequent lower values in the western Carolina high country (consistent with Parker and Ahijevych, 2007).

Shown in Table 3 is the seasonal cycle of the percentage of frozen precipitation relative to the total in each of the five regions. Two of the regions, western North Carolina and the Ohio Valley, have a significant frozen precipitation regime with 11.7 and 15.9% of winter season precipitation in solid form, consistent with the higher elevation, farther distance from the ocean, and more northerly latitude of those regions. Frozen precipitation makes up less than 1% of precipitation in the spring and autumn seasons, with a slightly higher percentage in the spring. The Florida panhandle had a trace amount of frozen precipitation in the winter and spring seasons, while the two ocean regions had no occurrence of frozen precipitation during any season.

Table 1. Frequency distribution of 2009–2012 daily-mean isolated precipitation values for the five 1° × 1° box regions illustrated in Figure 7.

Daily-mean isolated precipitation (mm day^{-1})	Gulf Stream off Carolina coast	Florida panhandle	Western North Carolina	Off Georgia coast	Ohio Valley
0–1	898	925	984	1016	1072
1–2	128	90	102	104	86
2–3	59	56	58	49	26
3–4	45	33	33	23	22
4–5	36	27	27	13	16
5–6	21	24	20	14	5
6–7	13	16	13	8	4
7–8	10	24	6	6	4
8–9	4	15	1	3	4
9–10	7	12	0	2	3
10–11	7	6	0	1	0
11–12	7	4	0	2	1
12–13	1	3	0	0	1
13–14	2	3	0	0	0
14–15	4	0	0	1	0
15–16	0	1	0	1	0
16–17	1	2	0	0	0
17–18	1	1	0	0	0
18–19	0	1	0	0	0
19–20	0	1	0	0	0

Table 2. Frequency distribution of 2009–2012 daily-mean MPF precipitation values for the five 1° × 1° box regions illustrated in Figure 7.

Daily-mean MPF precipitation (mm day^{-1})	Gulf Stream off Carolina coast	Florida panhandle	Western North Carolina	Off Georgia coast	Ohio Valley
0–10	1063	1140	1179	1186	1091
10–20	75	47	51	31	90
20–30	42	28	6	17	33
30–40	19	10	6	7	14
40–50	21	8	2	1	6
50–60	12	6	0	1	2
60–70	4	0	0	0	5
70–80	2	1	0	1	1
80–90	3	1	0	0	1
90–100	1	1	0	0	0
100–110	0	1	0	0	0
110–120	0	1	0	0	0
120–130	0	0	0	0	0
130–140	1	0	0	0	0
140–150	1	0	0	0	1

Table 3. The 2009–2012 seasonal fraction of frozen precipitation relative to the total, for the five 1° × 1° box regions illustrated in Figure 7.

% frozen precipitation	Gulf Stream off Carolina coast	Florida panhandle	Western North Carolina	Off Georgia coast	Ohio Valley
Winter (DJF)	0	0.02	11.7	0	15.9
Spring (MAM)	0	0.0015	0.85	0	0.53
Summer (JJA)	0	0	0	0	0
Autumn (SON)	0	0	0.06	0	0.40

4. Seasonal changes in diurnal cycle of MPF and isolated precipitation

Seasonal changes in the diurnal cycle of isolated and MPF precipitation across the SE USA give a revealing perspective on the modulation of local and larger-scale precipitation organization by the daily solar cycle.

Shown in Figures 14 and 15 is the seasonal variation of the three-hourly diurnal variation of isolated precipitation, for 2009–2012.

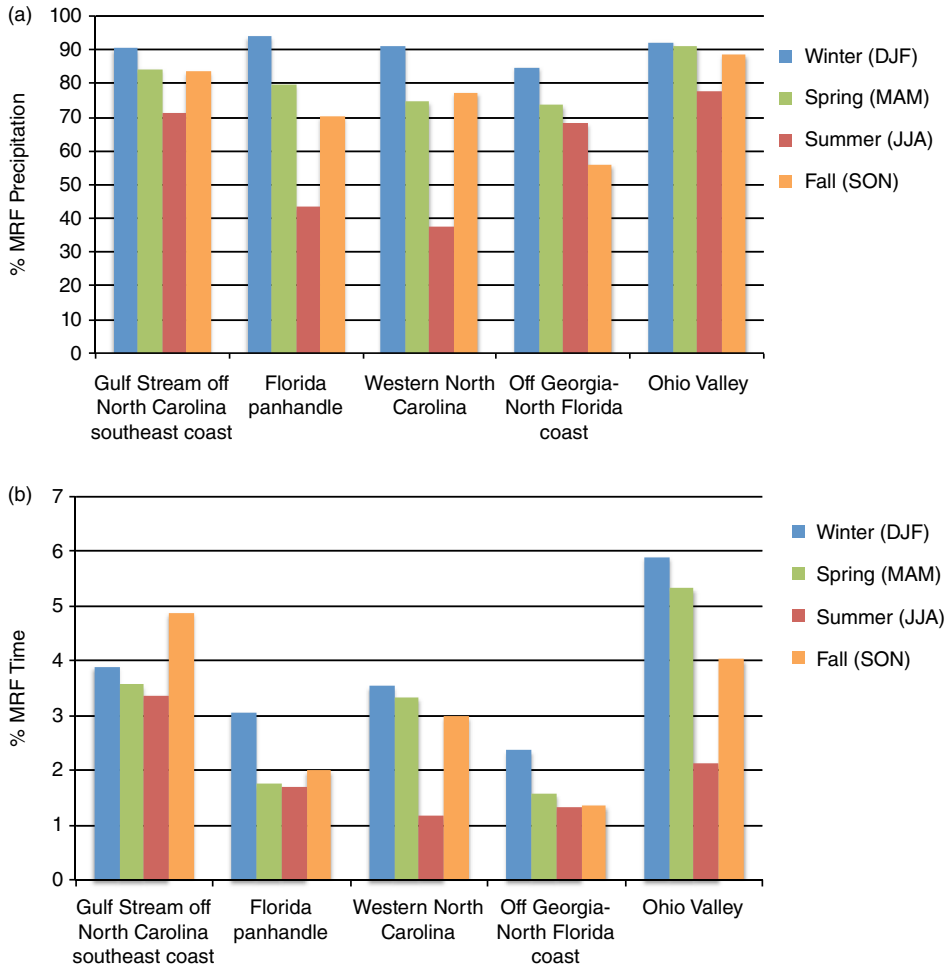

Figure 12. The 2009–2012 average seasonal variation of MPF within the five 1° × 1° boxes shown in Figure 7 for (a) % MPF precipitation relative to the total, and (b) % of the time MPF precipitation is present.

Not surprisingly, the greatest diurnal change occurs in the summer season (JJA), with essentially no diurnal variation during winter (DJF). In summer, the isolated precipitation preferentially forms offshore at night, increasing from just after midnight local time to a few hours after sunrise (0300–1200 UTC). The offshore nocturnal isolated precipitation clearly follows the outline of the coastal region, with the notable absence of nocturnal rain over the ocean just off the Georgia and north Florida coasts (box 4) discussed earlier. In the 3 h between late morning and early afternoon (1500–1800 UTC), the isolated precipitation dramatically switches from ocean to land, including Cuba and the Bahamas, clearly responding to daytime land surface heating. Inland, the isolated precipitation builds in the early afternoon, though is weaker away from the coast and northward. At 1800 UTC (Figure 15) there is a clear increase in isolated precipitation over the Appalachian high country in western North Carolina and eastern Tennessee, visible along the mountain ridges, likely related to thermally induced orographic circulations. The offshore isolated precipitation is weakening by 1800 UTC, but by 2100 UTC (late afternoon) offshore rain has mostly diminished while the inland has filled in over most land areas, particularly along the coastal plain. Around local sunset (0000 UTC) the land precipitation has begun to weaken. This diurnal evolution of precipitation aligns well with the radar analysis of Carbone and Tuttle (2008), who concluded that radar echo frequency was largest at 2100 UTC (late afternoon) across the Gulf Coast and southeastern coastal region, and increased offshore at night to an early–mid morning maximum (1300 UTC). They implicated the diurnal land–sea breeze circulation to explain that result, an interpretation consistent with the present study. The present result emphasizes that this diurnal rain variation is tied to isolated precipitation that increases in both frequency and intensity onshore during the day, with a reversed pattern at night. To the extent that isolated precipitation is locally generated, we conclude that there is a clear diurnal thermodynamic forcing in local precipitation in the summertime that reverses in phase between coastal land and ocean.

Figures 14 and 15 show that during the transition seasons of spring (MAM) and autumn (SON) the summer pattern is also evident in isolated precipitation, but at a lower intensity. Interestingly, while the increased afternoon isolated precipitation over land is similar in spring and autumn, the nocturnal rain over the ocean is greater in the autumn season where SSTs are 3–4 °C warmer along the Atlantic and Gulf coasts (not shown). This result is very likely due to the greater thermal inertia of the ocean compared to land, with warm coastal water generally persisting into the autumn season even after the advent of cold air advection into the southeast.

In contrast, there is no clear diurnal cycle of MPF precipitation (Figures 16 and 17) for much of the year except for summer. As with isolated precipitation, the greatest diurnal changes occur in the summer season (JJA), but with important regional differences not found in the isolated precipitation diurnal composites. The summertime MPF precipitation in the Ohio Valley in the northern domain has no diurnal pattern, suggesting that mesoscale and synoptic-scale precipitation is not modulated by diurnal heating and cooling, but likely by the essentially random timing of baroclinic system passage (e.g. Nieto-Ferreira *et al.*, 2013). In the coastal region, the warm season land–sea contrast also occurs with MPF precipitation, though not nearly as dramatically as with isolated precipitation. The summer MPF precipitation increases by 1800–2100 UTC, about 3 h after isolated precipitation, suggesting a transition from local to mesoscale organization as the afternoon progresses. With MPF precipitation, there is a clear regional difference in the diurnal timing of offshore rain. The Gulf Stream off the Carolina coast has a strong MPF rain

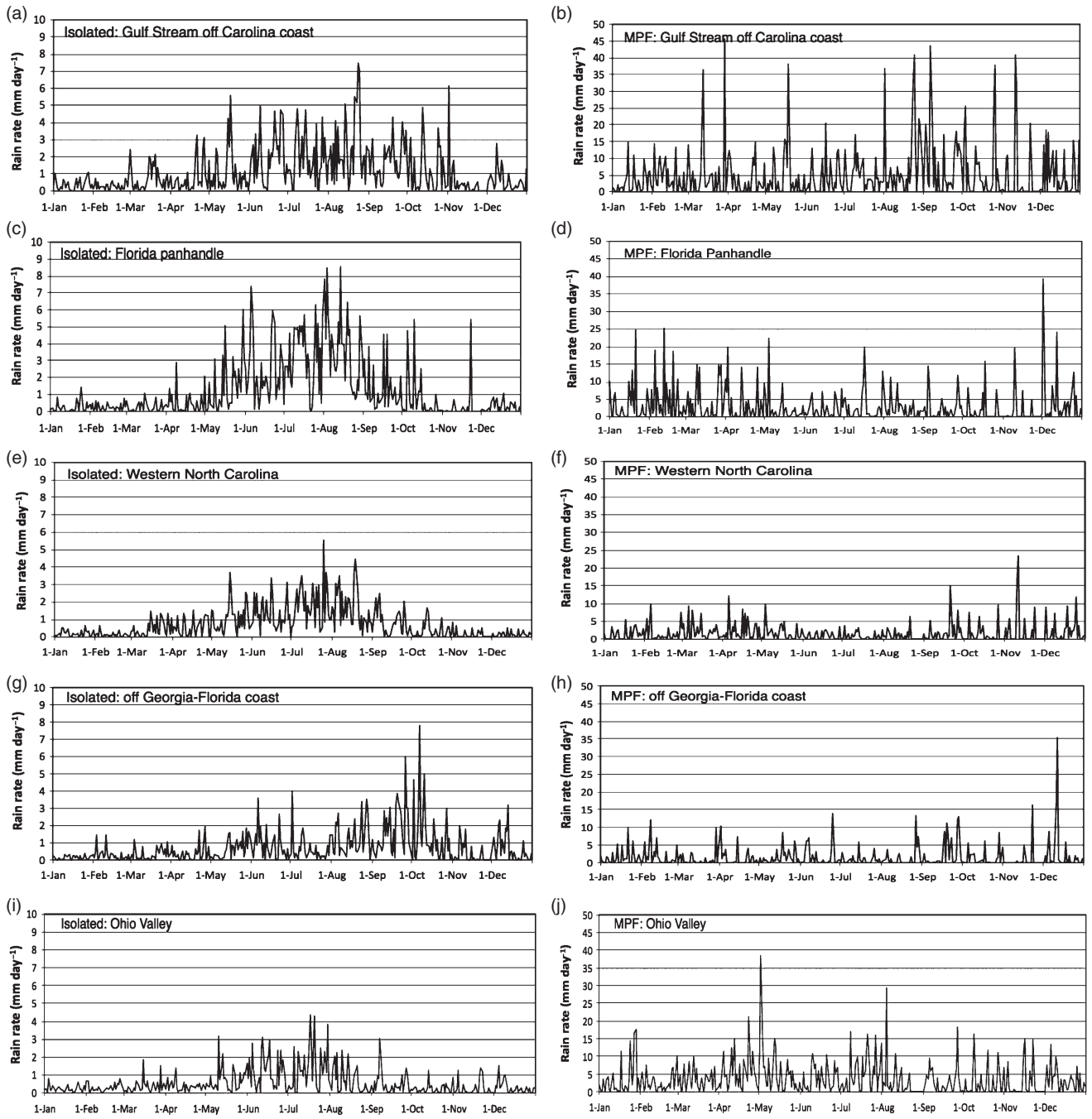

Figure 13. Annually averaged (2009–2012) time series of daily-mean isolated and MPF precipitation (mm day^{-1}) within the five 1° × 1° boxes shown in Figure 7. Time series plots are box 1 – Gulf Stream off Carolina coast for (a) isolated and (b) MPF; box 2 – Florida panhandle for (c) isolated and (d) MPF; box 3 – western North Carolina for (e) isolated and (f) MPF; box 4 – offshore Georgia and Florida coast for (g) isolated and (h) MPF; box 5 – Ohio Valley for (i) isolated and (j) MPF. Note that the vertical axis scale for MPF precipitation is 5× greater than that for isolated.

maximum in the early to mid-morning (0900–1200 UTC), while off the Gulf Coast the MPF maximum is several hours later (1500–1800 UTC). The reasons for the different diurnal timing of the ocean locations are not clear. Over land near the Carolina coast, the summertime MPF rain begins by 1800 UTC (early afternoon), expanding farther inland and intensifying over the next 3–6 h. This is very likely sea-breeze precipitation organized on the mesoscale, and is observed to largely diminish by 0300 UTC (late evening before midnight). The diurnal timing and location of the mesoscale sea-breeze precipitation along the Carolina coast is consistent with the detailed study of Koch and Ray (1997).

We can understand more about the mechanisms for the differences between coastal and offshore precipitation by focusing on the summertime diurnal variation of isolated and MPF precipitation in the vicinity of the Florida panhandle. Figure 18 shows the mean JJA diurnal variation of precipitation for the 1° × 1° region on the Florida panhandle coast, compared to a similarly sized region 100 km offshore over the ocean. This figure may be used to test the hypothesis (extending from Carbone and Tuttle, 2008) that on the western Florida Gulf coast, isolated convection forms onshore in the afternoon, organizes on the mesoscale, and propagates offshore in the evening (as found for coastal Panama systems by Mapes *et al* (2003)). Figure 18 shows that the maximum in isolated rain over land occurs about 3 h after the maximum in MPF rain over ocean, inconsistent with that hypothesis. Moreover, over the ocean, isolated precipitation has a maximum at 1200 UTC (just after sunrise) followed 3 h later by a maximum of ocean MPF precipitation, consistent with the formation and upscale evolution of offshore systems independently from land systems. Therefore the offshore precipitation likely forms and evolves independently of the land precipitation, suggesting diurnal changes in initiation of precipitation (for example by a land–sea breeze reversal) rather than the propagation offshore of a system formed earlier over land. Case-study analysis is under way to explore this relationship.

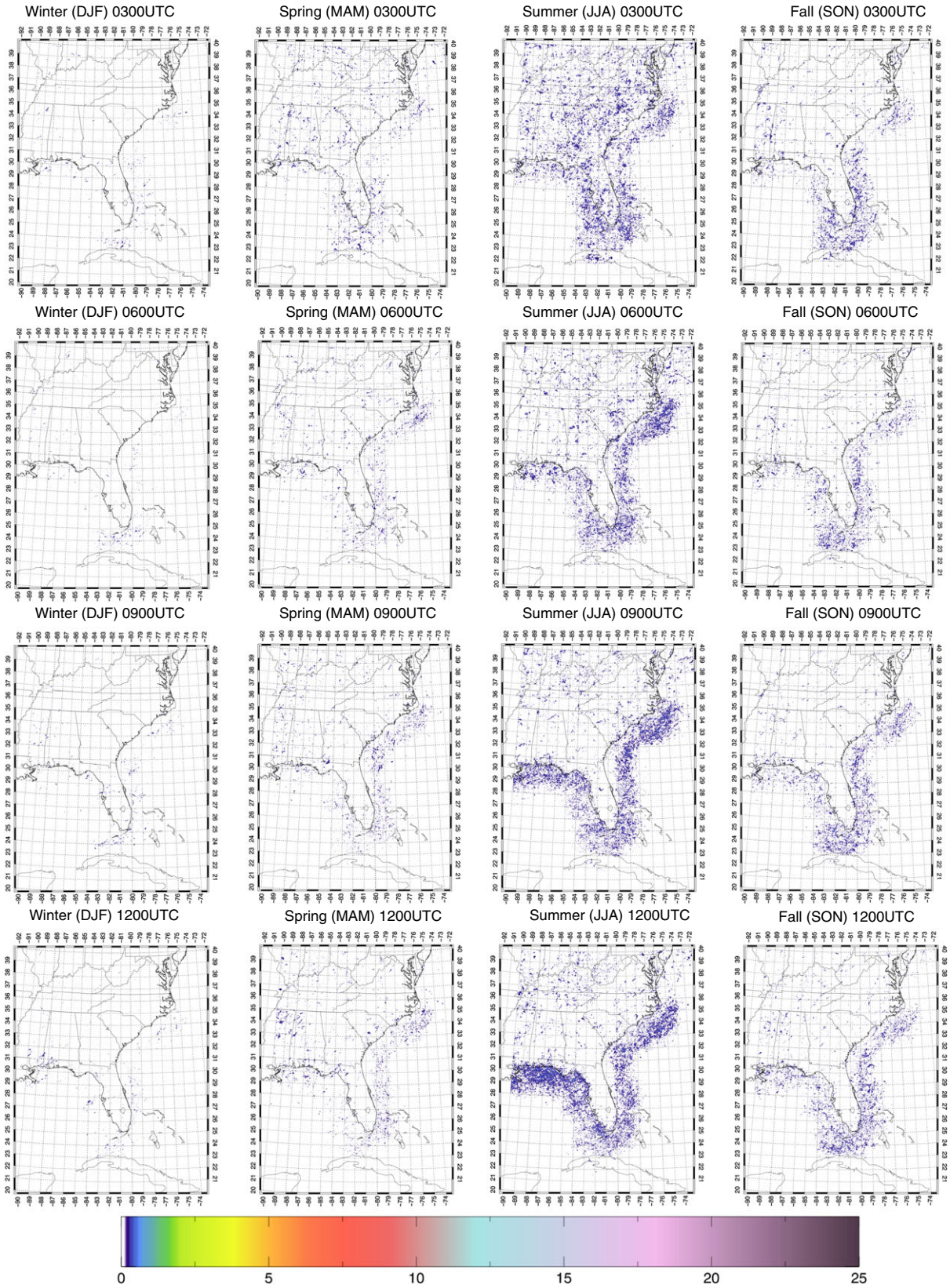

Figure 14. 2009–2012 averaged seasonal, three-hourly diurnal composite maps (mm h^{-1}) of isolated precipitation for 0300–1200 UTC. Eastern Standard Time (local time for most of the domain) is UTC minus 5 h.

5. Conclusions

A four-year (2009–2012) radar-based precipitation climatology of the SE USA, including seasonal and diurnal regional variations, was constructed using a simple framework of precipitation organization. Precipitation was classified into two categories of organization, mesoscale precipitation features (MPF) and isolated precipitation features. The aim is to determine whether and how the seasonal and diurnal variations of MPF versus isolated systems are distinct. The National Mosaic and Multi-sensor QPE dataset was analysed at 15 min intervals for four years over the SE USA from the Florida peninsula to the mid-Atlantic region, including the oceans within 200 km of the coast.

On average, 70–90% of precipitation is associated with MPF, generally less in the summertime and in southern coastal regions, with a relatively small seasonal cycle except in Florida and the warm offshore waters of the Gulf Stream. In contrast, isolated precipitation has a dramatic seasonal cycle that clearly outlines

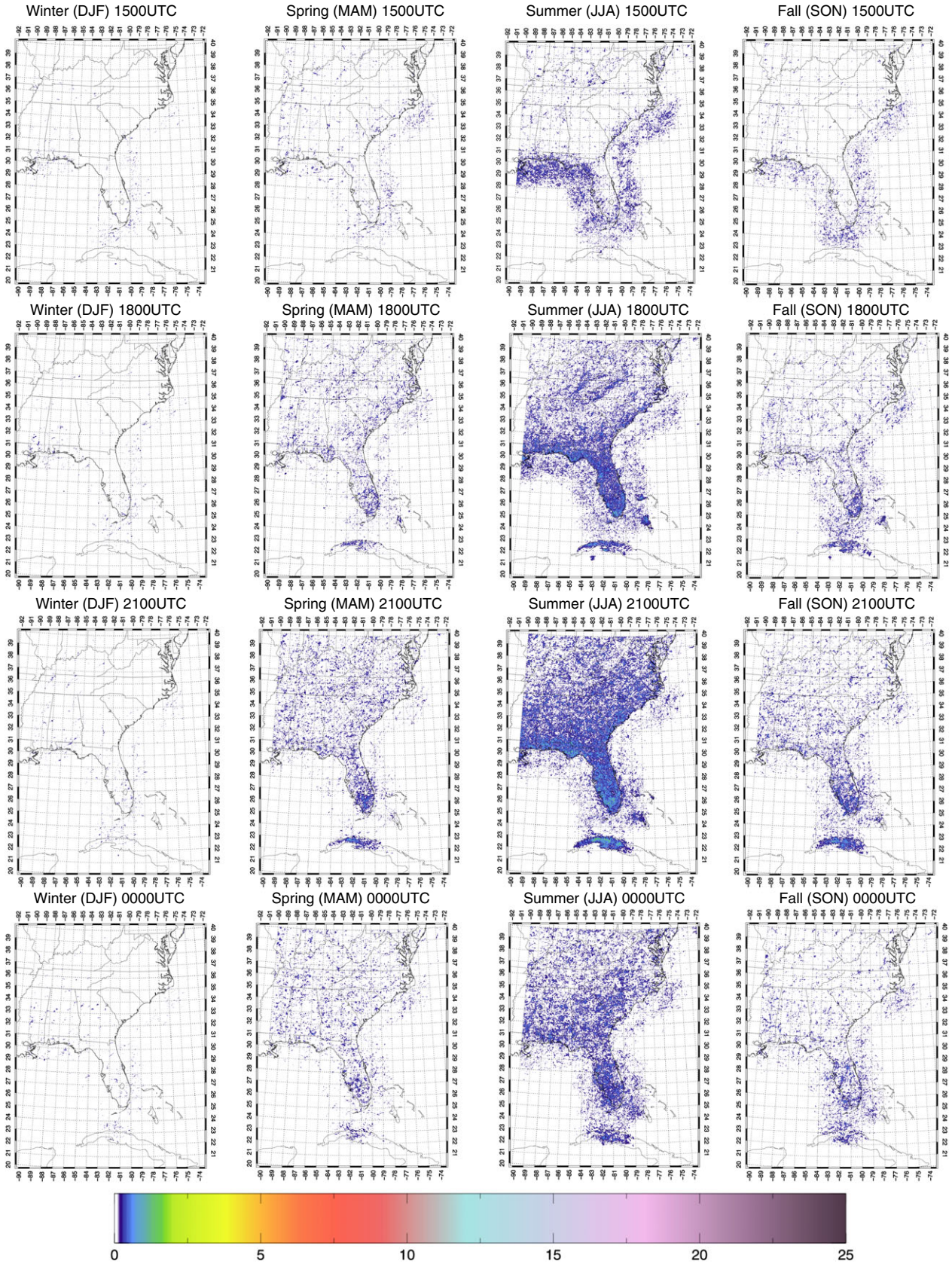

Figure 15. As in Figure 14 but for 1500–0000 UTC.

the SE coast in the summertime. Along the Florida panhandle, isolated rain makes up over half of summer rainfall, with a shift to higher extreme events in the frequency distribution of daily-averaged precipitation compared to the other regions. Isolated precipitation in the summertime therefore appears to be more thermodynamically driven, suggesting that isolated rain responds to surface heating either directly through high moisture content and thermodynamic instability, or indirectly through thermal circulations such as the sea breeze, or both.

Diurnal variations of MPF and isolated precipitation suggest clear distinctions in the mechanisms controlling the precipitation types. In summer, the isolated precipitation preferentially forms offshore at night, increasing from just after midnight local time to a few hours after sunrise. In the 3 h between late morning and early afternoon (1500–1800 UTC), the isolated precipitation rapidly and dramatically 'flips' from offshore to the coastal regions, including Cuba and the Bahamas, clearly responding to daytime land surface heating. By early afternoon there is a clear increase

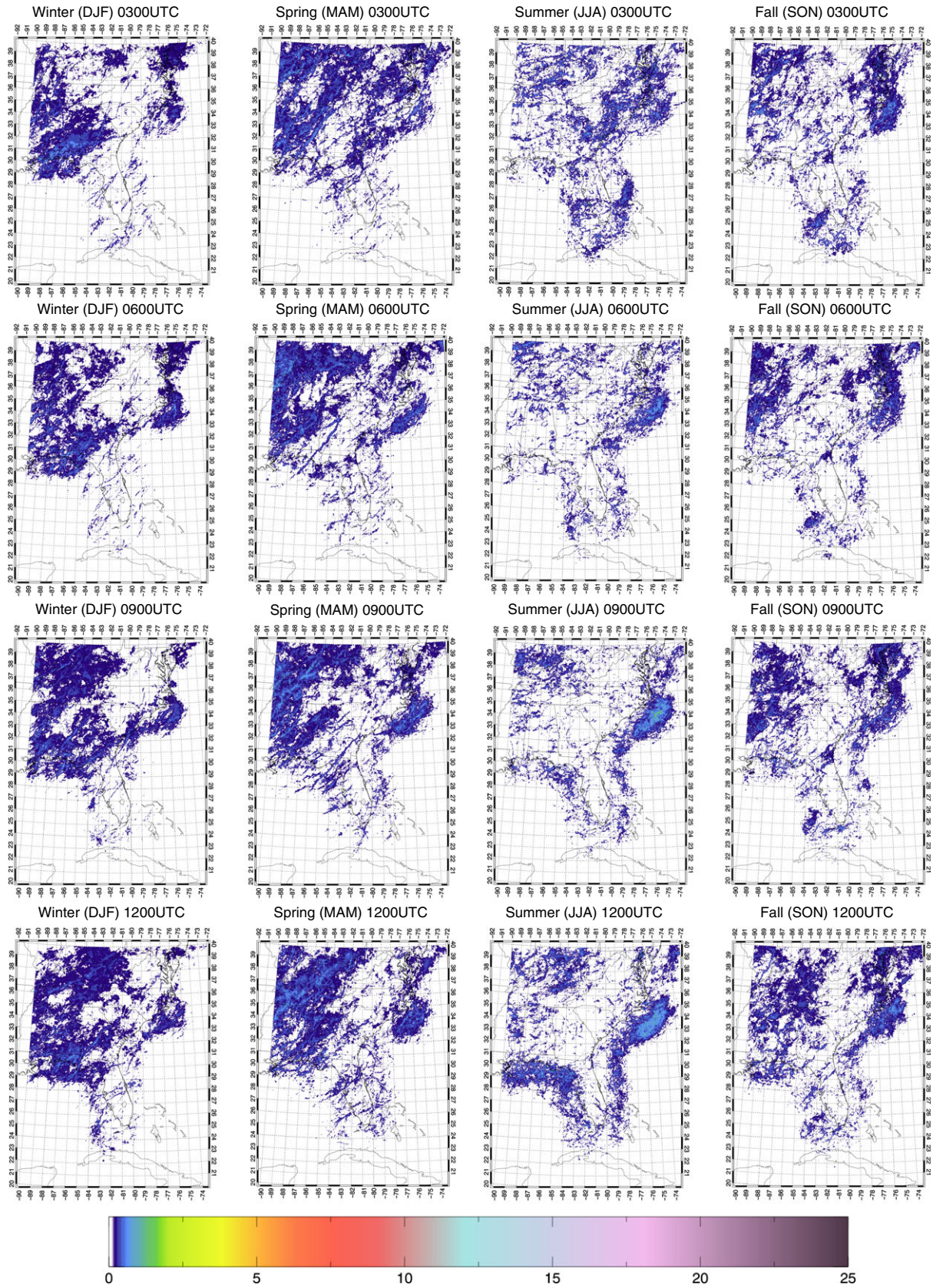

Figure 16. 2009–2012 averaged seasonal, three-hourly diurnal composite maps (mm h^{-1}) of MPF precipitation for 0300–1200 UTC. Eastern Standard Time (local time for most of the domain) is UTC minus 5 h.

in isolated precipitation over the Appalachian high country in western North Carolina and eastern Tennessee along the mountain ridges, likely related to thermally induced orographic circulations. In contrast, MPF precipitation has no clear diurnal variations except in the southern coastal region in the summer, likely associated with sea breeze convection organized on the mesoscale. In the Gulf Coast region of western Florida, offshore summertime precipitation likely forms and evolves independently of the land precipitation, suggesting diurnal changes in initiation of precipitation (for example by a land–sea breeze reversal) rather than the propagation offshore of a system formed earlier over land.

These results suggest that the MPF versus isolated precipitation system framework provides a useful basis for future studies of large-scale and local controls on precipitation and resulting implications for long-range predictability of precipitation.

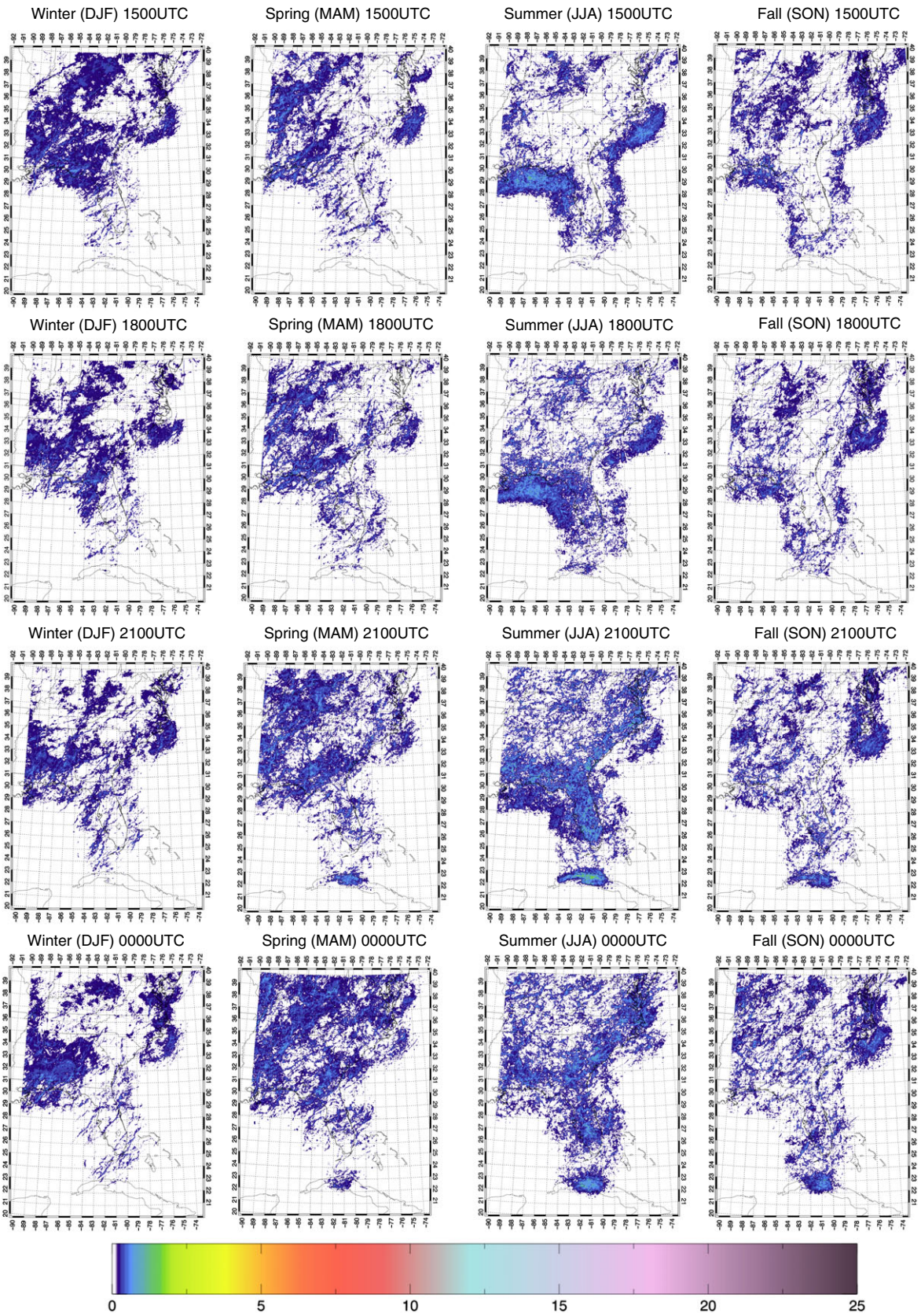

Figure 17. As in Figure 16 but for 1500–0000 UTC.

Building on the general results of this four-year MPF and isolated precipitation climatology, we plan to use the Weather Research and Forecasting (WRF) mesoscale model to investigate mechanisms for the different seasonal and diurnal behaviours of precipitation organization. We will also use WRF simulations to study potential changes in the precipitation organization climatology for future climate scenarios in Coupled Model Intercomparison Project phase 5 (CMIP5) projections. We also envision extending the precipitation climatology back to 1996, and perform interannual variability studies of regional and seasonal changes in the MPF and isolated precipitation across the SE USA.

Acknowledgements

This study was funded by a grant (AGS-1118141) from the National Science Foundation's Division of Atmospheric and Geospatial Science, both the Climate and Large-Scale Dynamics programme and the Physical and Dynamic Meteorology

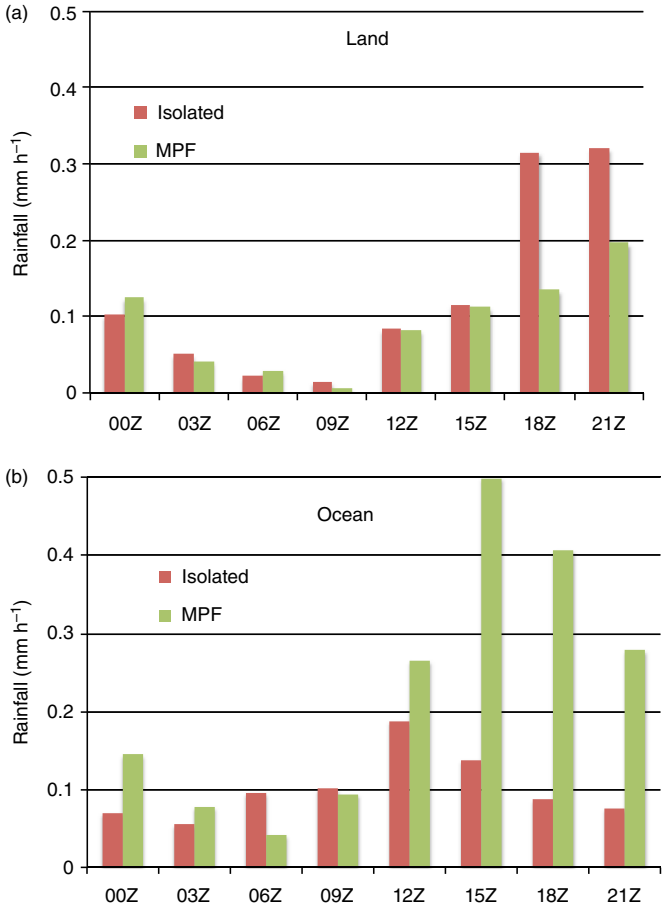

Figure 18. 2009–2012 mean summertime (JJA) diurnal variation of isolated and MPF precipitation (mm h^{-1}) for (a) 1° × 1° box over the coastal Florida panhandle (box 2 of Figure 7); (b) 1° × 1° box offshore of the Florida panhandle, 100 km due south of the land box.

programme. We appreciate the comments of the anonymous reviewers, which led to substantial improvements to the article. Gary Lackmann is gratefully acknowledged for useful discussions on the design of this study.

References

Alexander GD, Young G. 1992. The relationship between EMEX mesoscale precipitation feature properties and their environmental characteristics. *Mon. Weather Rev.* **120**: 554–564.

Ashley WS, Mote TL, Dixon PG, Trotter SL, Powell EJ, Durkee JD, Grundstein AJ. 2003. Distribution of mesoscale convective complex rainfall in the United States. *Mon. Weather Rev.* **131**: 3003–3017.

Carbone RE, Tuttle JD. 2008. Rainfall occurrence in the U.S. warm season: The diurnal cycle. *J. Clim* **21**: 4132–4146, doi: 10.1175/2008JCLI2275.1.

Carbone RE, Tuttle JD, Ahijevych DA, Trier SB. 2002. Inferences of predictability associated with warm season precipitation episodes. *J. Atmos. Sci.* **59**: 2033–2056.

Chao WC. 2013. Catastrophe-concept-based cumulus parameterization: Correction of systematic errors in the precipitation diurnal cycle over land in a GCM. *J. Atmos. Sci.* **70**: 3599–3614, doi: 10.1175/JAS-D-13-022.1.

Cheng C, Houze RA Jr. 1979. The distribution of convective and mesoscale precipitation in GATE radar echo patterns. *Mon. Weather Rev.* **107**: 1370–1381.

Gamache JF, Houze RA Jr. 1983. Water budget of a mesoscale convective system in the Tropics. *J. Atmos. Sci.* **40**: 1835–1850.

Geerts B. 1998. Mesoscale convective systems in the southeast United States during 1994–1995: A survey. *Weather and Forecasting* **13**: 860–869.

Hansen JW, Hodges AW, Jones JW. 1998. ENSO influences on agriculture in the southeastern United States. *J. Clim.* **11**: 404–411.

Houze RA Jr. 1989. Observed structure of mesoscale convective systems and implications for large-scale heating. *Q. J. R. Meteorol. Soc.* **115**: 425–461.

Houze RA Jr. 2004. Mesoscale convective systems. *Rev. Geophys.* **42**: 1–43.

Houze RA Jr, Smull BF, Dodge P. 1990. Mesoscale organization of springtime rainstorms in Oklahoma. *Mon. Weather Rev.* **118**: 613–654.

Kalnay E, Kanamitsu M, Kistler R, Collins W, Deaven D, Gandin L, Iredell M, Saha S, White G, Woollen J, Zhu Y, Leetmaa A, Reynolds R, Chelliah M, Ebisuzaki W, Higgins W, Janowiak J, Mo KC, Ropelewski C, Wang J, Jenne R, Joseph D. 1996. The NCEP/NCAR 40-year re-analysis project. *Bull. Am. Meteorol. Soc.* **77**: 437–472.

Koch SE, Ray CA. 1997. Mesoanalysis of summertime convergence zones in central and eastern North Carolina. *Weather and Forecasting* **12**: 56–77.

Konrad C. 1997. Synoptic-scale features associated with warm-season heavy rainfall over the interior southeastern United States. *Weather and Forecasting* **12**: 557–571.

Kuwano-Yoshida A, Minobe S, Xie S-P. 2010. Precipitation response to the Gulf Stream in an atmospheric GCM. *J. Clim.* **23**: 3676–3698.

Laing AG, Fritsch JM. 2000. The large-scale environments of the global populations of mesoscale convective complexes. *Mon. Weather Rev.* **128**: 2756–2776.

Leary C, Houze RA Jr. 1979. The structure and evolution of convection in a tropical cloud cluster. *J. Atmos. Sci.* **36**: 437–457.

McAnelly RL, Cotton WR. 1989. The precipitation life cycle of mesoscale convective complexes over the central United States. *Mon. Weather Rev.* **117**: 784–807.

Mapes BE, Warner TT, Xu M, Negri AJ. 2003. Diurnal patterns of rainfall in northwestern South America. Part I: Observations and context. *Mon. Weather Rev.* **131**: 799–813.

Mohr KI, Zipser EJ. 1996. Mesoscale convective systems defined by their 85-GHz ice scattering signature: Size and intensity comparison over tropical oceans and continents. *Mon. Weather Rev.* **124**: 2417–2437.

Nesbitt SW, Zipser EJ, Cecil DJ. 2000. A census of precipitation features in the Tropics using TRMM: RADAR, ice scattering and ice observations. *J. Clim.* **13**: 4087–4106.

Nesbitt SW, Cifelli R, Rutledge S. 2006. Storm morphology and rainfall characteristics of TRMM precipitation features. *Mon. Weather Rev.* **134**: 2702–2721.

Nieto-Ferreira R, Hall L, Rickenbach T. 2013. A climatology of the structure, evolution, and propagation of midlatitude cyclones in the southeast United States. *J. Clim.* **26**: 8406–8421.

Parker MD, Ahijevych DA. 2007. Convective episodes in the east-central United States. *Mon. Weather Rev.* **135**: 3707–3727.

Parker MD, Johnson RH. 2000. Organizational modes of midlatitude mesoscale convective systems. *Mon. Weather Rev.* **128**: 3413–3436.

Prat OP, Nelson BR. 2014. Characteristics of annual, seasonal, and diurnal precipitation derived from long-term remotely sensed data. *Atmos. Res.* **144**: 4–20.

Prat OP, Nelson B, Rickenbach T. 2010. 'A multi-sensor approach to access precipitation patterns and hydro-climatic extremes in the southeastern United States', Abstract H23K-03. In *Preprints, American Geophysical Union Fall Meeting*, San Francisco, CA.

Pritchard MS, Somerville RCJ. 2009. Assessing the diurnal cycle of precipitation in a multi-scale climate model. *J. Adv. Model. Earth Syst.* **1**: 12, doi: 10.3894/JAMES.2009.1.12.

Rickenbach TM, Rutledge SA. 1998. Convection in TOGA COARE: Horizontal scale, morphology, and rainfall production. *J. Atmos. Sci.* **55**: 2715–2729.

Schumacher C, Houze RA Jr. 2003. Stratiform rain in the Tropics as seen by the TRMM precipitation radar. *J. Clim.* **16**: 1739–1756.

Shepherd JM, Grundstein A, Mote T. 2007. Quantifying the contribution of tropical cyclones to extreme rainfall along the coastal southeastern United States. *Geophys. Res. Lett.* **34**: L23810, doi: 10.1029/2007GL031694.

Steiner M, Houze RA Jr, Yuter SE. 1995. Climatological characteristics of three-dimensional storm structure from operational radar and raingauge data. *J. Appl. Meteorol.* **34**: 1978–2007.

Wallace JM. 1975. Diurnal variations in precipitation and thunderstorm frequency over the conterminous United States. *Mon. Weather Rev.* **103**: 406–419.

Xu X, Howard K, Zhang J. 2008. An automated radar technique for the identification of tropical precipitation. *J. Hydrometeorol.* **9**: 885–902.

Zhang J, Howard K, Langston C, Vasiloff S, Kaney B, Arthur A, Van Cooten S, Kelleher K, Kitzmiller D, Ding F, Seo D-J, Wells E, Dempsey C. 2011. National Mosaic and multi-sensor QPE (NMQ) system: Description, results, and future plans. *Bull. Am. Meteorol. Soc.* **92**: 1321–1338, doi: 10.1175/2011BAMS-D-11-00047.1.

